ABSTRACT

TANG, CAN. Lithium Ion Battery Anodes Produced from Densified, Silicon Coated, Carbon Nanotube Arrays. (Under the direction of Dr. Philip Bradford.)

The increasing demand in energy storage for portable devices and electric vehicles requires the further development of lithium ion batteries. In this study, lithium ion battery anodes were produced from densified, silicon coated, carbon nanotube arrays. One of the goals of this study was to uniformly coat silicon onto individual carbon nanotubes. Carbon nanotube arrays were used to compensate for the volume expansion of silicon while providing the anode with sufficient electrical conductivity. A chemical vapor deposition system was built to synthesize carbon nanotube arrays and deposit the silicon coating. Baseline anodes of carbon nanotube arrays and silicon coated carbon nanotube array anodes were assembled and tested in coin cells without binder or a current collector metal foil. SEM, TEM, XRD and Raman spectroscopy confirmed relatively uniform crystalline silicon nano-particles were coated throughout the carbon nanotube arrays. The results showed that carbon nanotube array anodes with silicon coating had improved capacity as well as coulombic efficiency. Silicon coated post-treated carbon nanotube array anodes showed improved cycling performance with about twice capacity retention compared to the composite anodes produce with as-grown, pristine carbon nanotube arrays. After composite structure optimization, composite carbon nanotube array (chlorine+30%Si+carbon) anodes exhibited a charge capacity of 1360mAh/g for the first cycle with about 73% capacity retention on the 20^{th} cycle.

Lithium Ion Battery Anodes Produced from Densified, Silicon Coated, Carbon Nanotube Arrays

by
Can Tang

A thesis submitted to the Graduate Faculty of
North Carolina State University
in partial fulfillment of the
requirements for the Degree of
Master of Science

Textile Engineering

Raleigh, North Carolina

2012

APPROVED BY:

Dr. Saad Khan Member of Advisory Committee	Dr. Xiangwu Zhang Member of Advisory Committee

Dr. Philip Bradford
Chair of Advisory Committee

BIOGRAPHY

Can Tang was born on May 2nd, 1989, in Yangzhou, Jiangsu Province in China. After three years study in Yangzhou High School, she went to Donghua University to study textile engineering in September, 2007. In August, 2010, she joined the 3+X program provided by Donghua University and North Carolina State University and came to Raleigh, NC to continue the study in textile engineering. She got Bachelor of Science degree of Textile Engineering and Commerce in June 2010. From January 2010, Can started working as a research assistant with Dr. Philip Bradford on silicon carbon nanotube array anode for lithium ion batteries. After completing the program and getting Master's degree, she will start her career in textile related field.

ACKNOWLEDGMENTS

This research was made possible with many people's help. I would like to thank American Chemical Society and Textile Engineering, Chemistry and Science department for providing me with the chance to further my education in the textile engineering field. I would especially like to thank my advisor and chair, Dr. Philip Bradford, for his support and guidance all through the research. The encouragements he gave me are greatly appreciated. I will always remember that he taught me how to try to analyze and solve problems with a calm mind, which will benefit my life in the long run.

Also, I would like to thank my committee members: Dr. Xiangwu Zhang and Dr. Saad Khan. Their help and guidance were key to the completion of the project. Especially, I would like to thank Dr. Zhang for letting me use the equipment in the battery lab. The discussion with Dr. Zhang always helped deepen my understanding of the research field.

I would like to thank Ying Li for teaching me the knowledge and assembly of battery. Also, I would like to thank Kelly Stano, who is an excellent lab partner. I would like to extend the thanks to all the people in the battery lab.

Finally, I would like to thank my parents. They always encourage me with all their love and warmth.

TABLE OF CONTENTS

LIST OF TABLES

LIST OF FIGURES

1. Introduction

In today's communication dependent society, lithium ion batteries have become the major choice and trend for portable electric devices and light-weight energy storage materials. Compared with Ni-MH, and Ni-Cd batteries, energy densities of lithium ion batteries are almost two times higher as seen is Figure 1.1. However, the application of lithium ion batteries in automobile industry is limited due to high cost, low durability and especially relatively low energy densities. Electric vehicle batteries lithium ion battery packs should be as small and light as possible to be space and energy efficient while providing satisfactory energy storage ability.

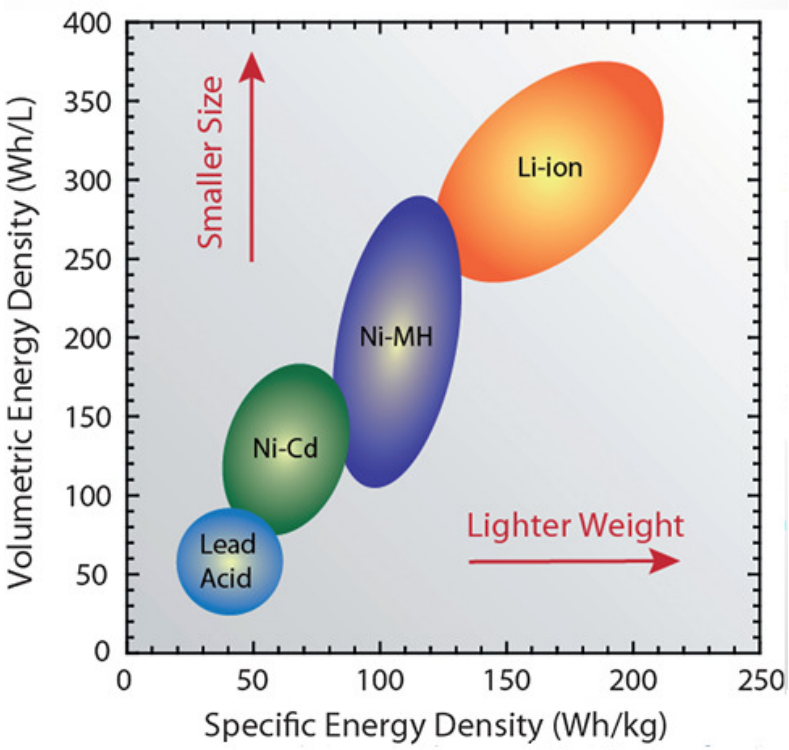

Figure 1.1 Comparison of rechargeable battery technologies [1].

One important aspect to improve lithium ion batteries is to improve the energy density of the anode. Graphite has a relatively low theoretical capacity of about 372 mAh/g, which is the current commercial anode material. People have turned to other materials to achieve higher capacity. Among them, silicon has been seen as potential lithium ion battery anode material for its extraordinary theoretical capacity of about 4200mAh/g. However, volume expansion up to 300% can appear during lithium insertion and extraction. Efforts have been made to make use of silicon as anode material for lithium ion battery while accommodating for the structural instability during cycling. To stabilize the structure of silicon and improve electric conductivity, carbon-based materials have been widely used in lithium ion battery anodes. Among all kinds of carbon-based materials, carbon nanotubes are ideal to combine with silicon. Carbon nanotubes can provide silicon with great buffer for volume expansion with their outstanding mechanical properties. The low electrical conductivity of silicon can also be compensated by carbon nanotubes.

The motivation of this research study is to utilize the extraordinary mechanical properties and conductivity of carbon nanotube arrays to help accommodate the stress build-up and release of silicon in lithium ion battery anodes. Chemical vapor deposition (CVD) will be used to synthesize carbon nanotube arrays and deposit silicon onto the arrays. The composites will be shear pressed into thin sheets to use as anode materials directly. Since the anode will not have current collector or binder, the energy density of the test cell is expected to be high. More importantly, the anodes should have good cycling performance with relatively high capacity.

This thesis includes construction of the CVD system and optimization of carbon nanotube array growth. Si deposition on carbon nanotube arrays in the CVD system will be studied. To examine the properties of the fabricated anodes, morphology characterization as well as electrochemical tests results are presented.

2. Literature review

2.1 Carbon nanotubes

2.1.1 Carbon nanotube structure and properties

Since the report in 1991 by Sumio Iijima, carbon nanotubes have opened an entirely new area for research and industry. Their excellent and unique properties make them one of the most exciting materials in the 21st century. Carbon nanotubes are wrapped coaxial graphitic sheets with high length to diameter ratio. The change in dimensions and layers of the graphitic sheets lead to different types of carbon nanotubes. Single-walled carbon nanotubes (SWCNT) and multi-walled carbon nanotubes (MWCNT) are the major divisions of the carbon nanotube family. Multi-walled carbon nanotubes have many concentric wrapped graphene layers while single-walled carbon nanotubes are single rolled graphene sheets.

Carbon nanotubes have extraordinary mechanical, thermal and electric properties. Due to the sp^2 bonding, carbon nanotubes have extremely high strength and modulus. The thermal conductivity is high along the tube length, showing "ballistic conduction", but quite low perpendicular to the axial direction. The electric properties of single-walled carbon nanotubes depend on the structure and symmetry of the graphitic layer. A pair of indices (n,m) characterizes the way in which the graphene sheet is wrapped. If n=m, the carbon nanotubes are metallic; otherwise, the carbon nanotubes are semi-conductive [2]. Multi-walled carbon nanotubes are mostly conductive and often contain more defects

compared with single-walled carbon nanotubes. The electrochemical properties are especially important since this study focuses on lithium ion battery anode material fabrication. It will be discussed in detail in section 2.3.

The various arrangements of the carbon nanotubes can present unique properties and benefits as well. Carbon nanotubes used to be very short. With the ability to produce long, high aspect ratio carbon nanotubes, forming 2D or 3D structured has increased popularity. Vertically aligned carbon nanotube arrays [3], carbon nanotube yarns [4], carbon nanotube sponge [5], carbon nanotube buckypaper [6] and other structures all show great potential in a wide range of areas. Among them, vertically aligned carbon nanotube arrays are preferred in many situations due to their inherently aligned structure. The carbon nanotube arrays can behave like springs with excellent elastic energy storage ability. Also, composites can be made with controllable structure which may fully utilize the mechanical properties along the length of carbon nanotubes. Electric applications favor aligned carbon nanotubes as well.

2.1.2 Carbon nanotube production

Technologies such as arc discharge, laser ablation and chemical vapor deposition have been developed to synthesize carbon nanotubes. With the progress in catalyst and process, mass production of carbon nanotubes has become more promising.

Carbon nanotubes were first produced on the negative end of carbon electrode using arc

discharge method, which can produce high quality single- and multi-walled carbon nanotubes under high temperature [7]. Laser ablation uses a pulsed laser to vaporize a graphite target, fabricating mostly single-walled carbon nanotubes with controllable diameter [8]. Chemical vapor deposition (CVD) has been popular to synthesize carbon nanotubes for many years. It mainly yields multi-walled carbon nanotubes with relatively lower quality, but less cost. Traditionally, carbon nanotubes are grown on metallic substrates with pre-deposited layers of catalyst [9]. By using different carbon precursor, the carbon nanotubes can have varied structure and properties. Recently, several groups have improved the method through using a floating catalyst process [10]. The improved chemical vapor deposition method eliminates the inconvenience of pre-deposition and has the ability to produce millimeter long carbon nanotubes. The yield and the growth rate of the improved method are much higher than the old one, showing the potential for mass production. By introducing growth-enhancing components such as chlorine, carbon nanotubes can be spun at high speed into yarns, which is very promising for future applications.

2.2 Lithium-ion batteries

With the development of renewable energy, finding a reliable way to store energy has become more and more important. Lithium ion batteries have advantages such as high energy density, no memory effect and low self-discharge. A typical lithium-ion battery has the anode and cathode partitioned by a separator with electrolyte filling the empty

space as shown in Figure 2.1.

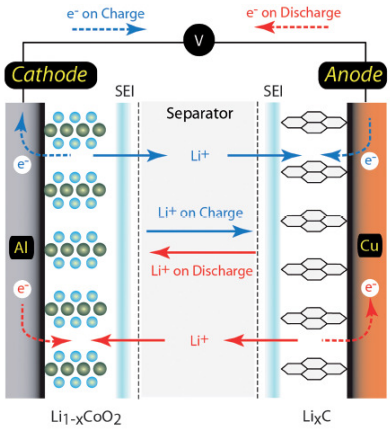

Figure 2.1 Structure of a traditional lithium ion battery [1].

The positive electrode half reaction [1]:

$$\mathrm{LiCoO_2} \leftrightarrows \mathrm{Li_{1-x}CoO_2} + x\mathrm{Li^+} + x\mathrm{e^-}$$

The negative electrode half reaction:

$$x\mathrm{Li^+} + x\mathrm{e^-} + 6\mathrm{C} \leftrightarrows \mathrm{Li_xC_6}$$

The total capacity of the lithium ion battery in relationship with anode and cathode capacity is as following equation, where C_A and C_C are the theoretical specific capacities of the anode and cathode material, and $1/Q_M$ is the specific mass of other cell components :

$$\text{Total cell } (\mathrm{mAh\,g^{-1}}) = \frac{1}{(1/C_A) + (1/C_c) + (1/Q_M)} = \frac{C_A C_C Q_M}{C_A Q_M + C_C Q_M + C_A C_C} \quad [11]$$

2.2.1 Anode

The stability of the anode structure affects the cycling performance of battery. Lithium ions insert into anode during charge and extract out during discharge. The ability of the anode to store lithium-ions plays a crucial role in the capacity of the battery. The ideal anode should have low irreversible capacity, high reversible capacity, stable cycling behavior and good rate performance. Also, the anode is expected to be easily fabricated and compatible with all other parts of the system.

The most popular commercial anode material is graphite. Other forms of carbon such as pyrolized carbon and carbon fiber are also available in the market. Materials under development include nanomaterials, and silicon composites. The design of the battery structure as well as material combination have been a prevalent area of research over the decades.

2.2.2 Cathode

In a lithium ion battery, lithium ions extract from cathode during charge and insert in during discharge. As the lithium ion source, the cathode is expected to have high lithium storage capacity. In addition, the cathode should be able to release and receive lithium ion efficiently during cycling.

The popular cathode material covers $LiCoO_2$, $LiMn_2O_4$, $LiNiO_2$ [12] and etc. Compared with the optimization of structure of anode material, the development of cathode

materials has mainly focused on the choice of materials [12].

2.2.3 Separator

The anode and cathode is separated by a microporous separator which prevents the contact of electrodes while allowing ions to pass through. Separator materials include nonwovens, polymer films and natural substances [13]. For lithium ion batteries, polypropylene(PP) and polyethylene(PE) films are common separator materials.

2.2.4 Electrolyte

The electrolyte in a lithium ion battery provides ions for the chemical reaction to reversibly to take place. It is comprised of lithium salts such as $LiPF_6$, $LiBF_4$ in organic solvents such as ethylene carbonate, dimethyl carbonate and diethyl carbonate [14]. The electrolyte forms a solid electrolyte interface (SEI) on anode surface during the initial charge. Formation of the SEI leads to part of the irreversible capacity while also preventing further decomposition of the electrolyte.

2.2.5 Binder

Traditionally, the active material, a binder and additives are made into slurry and applied onto the current collector. The binder plays an important role in holding the electrode material together and helping maintain contact with current collector. Polyvinylidene Fluoride (PVDF) is currently the most popular binder for cathodes and anodes in lithium ion batteries [15]. The binder should achieve certain extent of purity to avoid side reactions. Meanwhile, the binder needs to be compatible with the battery system.

2.2.6 Current collector

In most cases, the current collector is needed to improve the transfer of electrons. Usually, aluminum foil is used for cathode and copper foil for anode. Though it is a crucial part of the battery, the current collector can be heavier than the electrode material due the high densities of metallic material. For example, the current collector takes about 12.8% weight percent of the whole battery in the high power cell while the active material and binder only takes about 4.3% weight percent [16]. If the current collector mass is decreased, the energy density of the entire battery will increase.

2.2.7Additives

To improve the electrical conductivity of the electrodes, carbon black, carbon nanotubes or some other conductive materials are added during fabrication. The additives not only add to the weight of the electrodes, but also can have effect on the properties since they are electrochemically active.

Additives can have other benefits such as inhibiting the formation of SEI, enhancing the deposition of Li, helping to protect the cathode and can help improve the safety [17].

2.3 Carbon based materials for lithium ion batteries

With graphite as the commercial anode material, carbon-based materials are well known for their good conductivity and small volume expansion upon lithium intercalation. The

theoretical specific capacity of carbon-based material is about 372mAh/g according to Faraday's law:

$$x\ Li+ + x\ e + 6\ C \leftrightarrow LixC_6 \quad (0<x<1)\ [18]$$

However, the obtained capacity in reality is dependent on many factors. The traditional graphite alone cannot meet the increasing demand for fast charging high energy density batteries. Advanced carbon-based materials have been explored to make anode materials with high performance.

2.3.1 Graphite

Graphite is the major choice for today's market lithium ion battery anode. Both natural and synthetic graphite are used for the application. The main advantage of graphite anode lies in cycling performance; up to 1000 cycles can be achieved with low capacity loss [19]. The lithium intercalates through the graphene layers during charge and discharge as shown in Figure 2.2. The SEI layer formation in the first cycle leads to irreversible capacity. Since graphite intercalates with lithium at very low voltage as 0.2V, it is possible for clusters of lithium to be formed if slight over-potential occurs during rapid recharging. This will eventually lower the capacity [20].

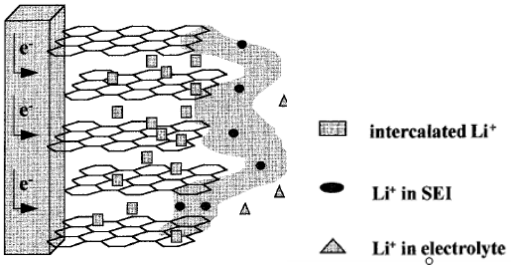

Figure 2.2 Lithium intercalation in graphite anode [21].

Experiments have been done to modify the surface or to make it into composite in order to get better properties. However, graphite has low practical specific capacity and low maximum working voltage.

2.3.2 Carbon nanofiber

Carbon nanofibers are cylindrical micro-structured carbon material. When applied as anode material, lithium ions insert and extract from the surface of the carbon nanofiber to the inside during charge and discharge. The structure can be made porous by separating components during fabrication. The common methods to produce carbon nanofibers are pyrolysis of carbon precursor, which is usually pitch or polyacrylonitrile (PAN), and chemical vapor deposition. Pyrolysis of electro-spun fibers has been widely used recently since the structure is more predictable through controlling the spinning parameters such temperature and voltage. Besides the good mechanical properties, the main advantage of carbon nanofibers is that they can be used as carrier materials for inorganic anode materials such as silicon and tin, as well as conductive material in the battery. The advanced anode material made with carbon nanofiber composites can combine the cycling property of carbon material and the high specific capacity together. Carbon nanofibers can be packed closely to produce a nonwoven structure (Figure 2.3), giving it the potential to eliminate the need for current collector.

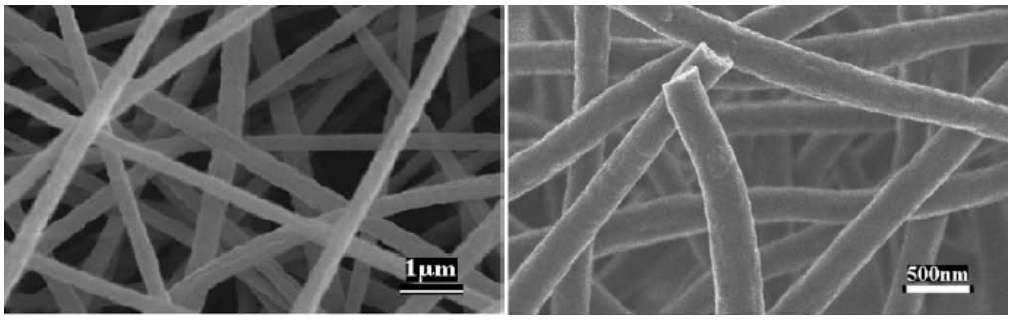

(A) (B)

Figure 2.3 FESEM images of (A) untreated PAN nanofibers and (B) thermally treated CNFs [22].

2.3.3 Carbon nanotube array

Because of the excellent mechanical properties, carbon nanotubes have been used as matrix in anode composites to e buffer for materials which has high potential capacity but dramatic volume expansion upon lithium intercalation. It is also commonly used with other cathode material as well to increase conductivity [18]. For the case of lithium ion battery anodes, multi-walled carbon nanotubes are mostly used for good electrical conductivity. Single-walled carbon nanotubes still have problems with purity and defects in the case of lithium ion battery application. The carbon nanotubes can be in the forms of powder, random network and arrays. Among these, the carbon nanotube arrays show high capacity, great rate performance and stable cycling property. These "forests" feature carbon nanotubes that are parallel to each other, and are mutually supported by the surrounding array. Figure 2.4 shows a well aligned carbon nanotube array.

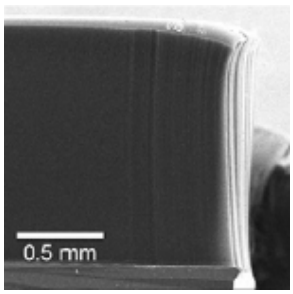

Figure 2.4 An example of carbon nanotube array [23].

Carbon nanotube arrays were found to exhibit high capacity and better performance compared with entangled carbon nanotubes [24] as shown in Figure 2.5. The end of carbon nanotubes can be closed up when the growth stops. The end caps of the carbon nanotubes were removed upon cycling, accommodating further lithium intercalation [24]. The highly aligned nature of carbon nanotubes within the array provided the lithium ions with shorter lithium path way and better conductivity. Additionally, lithium ions would intercalate at the end of the carbon nanotubes, in the outer graphene layer as well as in the defects as shown in Figure 2.6. The carbon nanotube array is very promising for nonorganic material deposition as well, due to the very high surface area.

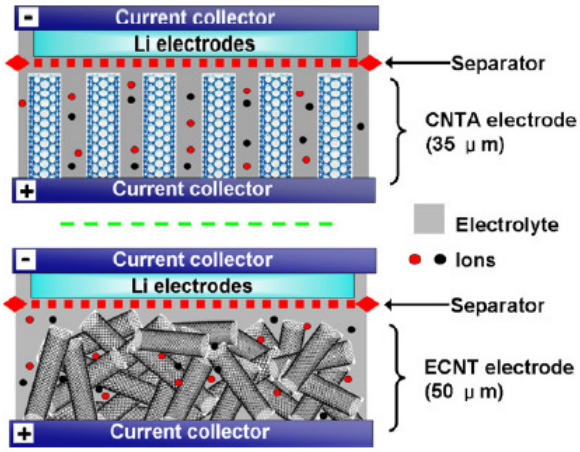

Figure 2.5 Carbon nanotube array versus entangled carbon nanotube anodes [24].

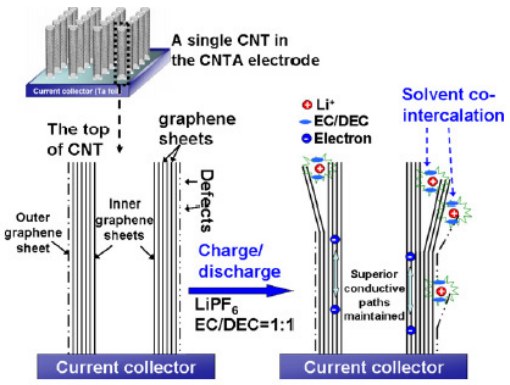

Figure 2.6 Lithium intercalation in carbon nanotube array [24].

Usually, the carbon nanotube arrays are attached to a current collector either by transfer method or one step grow method. The advantage of one step grow method which has carbon nanotube arrays directly grown on the current collector is the stronger connection to substrate and lower electric resistance due to better contact with current collector.

The cyclic voltammetry (CV) test result of carbon nanotube array anodes in Figure 2.7 showed a rectangular and symmetric curve, indicating good rate performance [25].

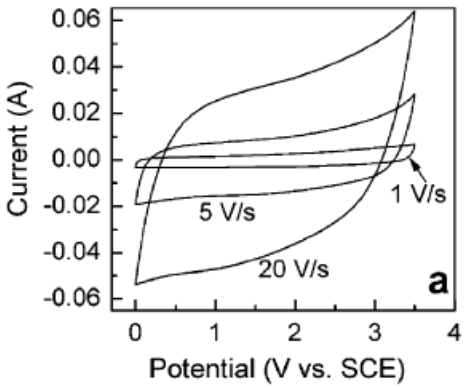

Figure 2.7 CV curves of carbon nanotube array anode battery [25].

To further improve the electrochemical performance of carbon nanotubes, opening the end cap and side wall vacancies have attracted the attention of researchers, which can let lithium ions insert through the side walls. The " cutting" effect can be achieved through selective oxidation by acid solution or ultra-sonication [1].

A major issue in the utilization of carbon nanotubes is the variation from batch to batch and among different labs. Parameters such as temperature, pressure, time and carbon precursor are important for the properties of the produced carbon nanotube. The effects of growth temperature for carbon nanotubes considering structure and electrochemical properties were investigated by Wu and *et al*. The electrochemical test results of carbon nanotubes grown at three different temperatures indicated that the first charge capacity of the carbon nanotubes decreased with the increase of preparation temperature [26]. In the growth of carbon nanotubes, the goal is to maintain the optimized conditions constant each run to guarantee the consistency of the obtained carbon nanotube as anode material, thus minimizing the fluctuations of battery properties caused by material production.

2.4 Inorganic materials for lithium ion battery anode

In the pursuit of high energy density batteries, anode researchers have turned to materials that can store more lithium ions than traditional carbon based anode materials. The diagram seen in Figure 2.8 gives a list of materials used in lithium ion battery electrodes. It indicates that inorganic materials such as silicon, tin and germanium have much higher

energy density than carbon based anode materials.

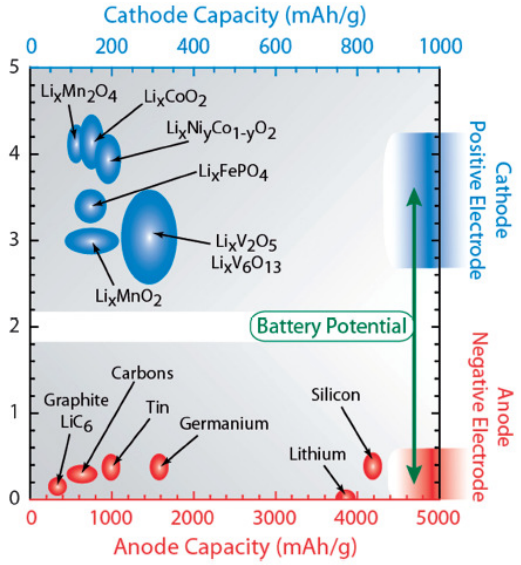

Figure 2.8 Material comparison in capacity and potential [1].

However, the problem with those elements lies in severe volume expansion upon cycling. For example, aluminum has a potential capacity as high as 2235mAh/g, but the volume expansion goes up to 238% [18], resulting in dramatic capacity fading. One strategy to solve the expansion problem is to scale down the size of those materials into the nano-range and incorporate with a carbonaceous matrix.

2.4.1 Silicon as an energy storage material

As seen in Figure 2.8, silicon shows the highest potential specific capacity of about 4200mAh/g when forming the lithium alloy Li_4Si. However, the volume expansion, up to 300%, is something researchers must solve to make silicon a realistic material for future lithium ion batteries.

During lithium insertion and extraction, the dramatic changes in strain and stress change leads to a large volume expansion of the silicon anode, resulting in pulverization of the structure into cracks and disintegrated pieces. The SEI layer formed in the initial charge can break into the battery system and new layer has to be formed each time, leading to irreversible capacity each cycle. With repeated strain and stress changes induced by cycling, the silicon anode can be pulverized, leading to loss of contact with the current collector and more severe capacity fading as seen in Figure 2.9. Even if the silicon is in particle form, the same problem exists. As the initial morphology is destroyed, the particles will eventually lose electrical contact, again leading to capacity fading.

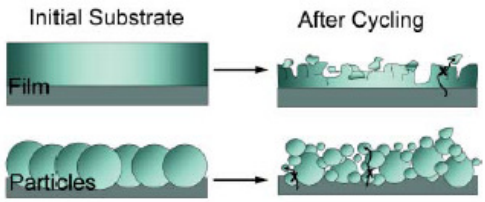

Figure 2.9 Silicon film and particles as lithium ion battery anodes [20].

Besides the volume change, it is observed in many cases that crystalline silicon becomes amorphous upon cycling. In Obrovac's study, fully lithiated amorphous silicon became highly crystalline at 50mV with the second phase of $Li_{15}Si_4$ [28]. The delithiation of the phase $Li_{15}Si_4$ lead to the change of crystalline phase to amorphous phase. To reduce the effect, cycling above 50mV was proven to improve the cycling property of the silicon anode [27].

Numerous methods to improve the cycling behavior of silicon anodes have been explored.

One method is to make silicon nanowire and nanotubes. However, the low packing density and still low cycling behavior means this method needs further development [28]. The other direction is to make silicon composite anode. The nano-sized silicon particle anode can help improve the cycling, but the capacity fading will still be severe. To prevent cracking and disintegration, the silicon nano particles are desired to be dispersed in a ductile matrix with high plastic deformation ability [11], which can compensate for the large volume expansion.

2.5 Silicon and carbon based composite materials for lithium ion battery anodes

To improve the cycling performance of silicon anodes, carbon based materials, especially carbon nanotubes, are used as matrix for silicon. Carbon based materials have good mechanical properties to accommodate stress and strain change in silicon. They are also highly electrochemically conductive and active. To utilize the flexibility of carbon nanofibers and carbon nanotubes, various silicon-carbon composite structures have been designed for a lithium ion battery anode. The designed composites fall in three main categories: mixed structure, carbon coated silicon and silicon coated carbon. There are also some complex designs such as scaffold and multi-layer structures.

2.5.1 Mixed structure

The mixed structure is probably most explored structure, which often includes a mixing process to reduce the size of raw materials and disperse silicon particles in the carbon or carbon precursor. Then the mixed materials are prone to pyrolysis or other reduction

methods to achieve a silicon-carbon mixture. The obtained silicon-carbon mixture is slurry pasted on the current collector to make the anode. It is found that the surface area and porosity of the anode material as well as the charge transfer resistance play an important role in performance [29].

A common way to prepare silicon-carbon composites is ball milling silicon and carbon with binder and additives. Eon et al. have used ball milling to make a silicon-multi-walled carbon nanotube composite [30]. Scanning Electron Microscopy (SEM) images in Figure 2.10 showed that the multi-walled carbon nanotubes encapsulated the Si powders more tightly and evenly with 1:1 MWCNT and Si loading. The 1:1 ratio anode also exhibited the lowest irreversible capacity and highest reversible capacity in all tested anodes, with a first cycle charge capacity of 1770mAhg-1 [30]. However, there still appeared to be big clusters of silicon which was prone to fracture during cycling.

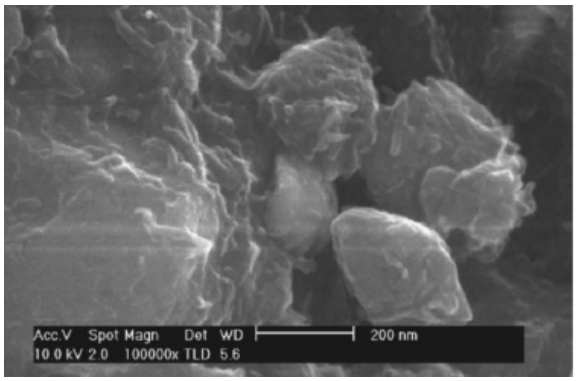

Figure 2.10 Silicon and multi-walled carbon nanotube composite [30].

Another way to prepare the composite is through pyrolysis or reduction of the milled silicon-carbon precursor mixture. In Jin et al 's study, Si/CNFs composite anode materials

were obtained from carbonization of Si/PAN and Si/PAN/PLLA electrospun nanofibers [31]. The non-woven fibrous structure films with bead like silicon particles throughout were attached to copper foil directly as an anode. The anode with PLLA as the conductive material showed better electrochemical performance, exhibiting more than 700mAh/g discharge capacity in the fortieth cycle [31]. Inactive materials can be added during milling as well. For example, nanosized Si was prepared by mechanochemical reduction of SiO by aluminum, which was ball milled with graphite to achieve a uniform dispersion. The battery exhibited stable capacity around 500mAh/g, which was due to the buffer provided by inactive Al oxides and graphite [32].

The chemistry of the composites was characterized through a variety of methods. X-ray Diffraction (XRD) was used to verify the insertion of lithium ions during various stages of electrochemical tests. It was confirmed that lithium ions inserted into the graphene layers of multi-walled carbon nanotubes during charging, which was due to increased open ends introduced by ballmilling and alloying with Si. In-situ Raman microscopy was used to study the first discharge cycle of a mixed monocrystalline silicon and carbon anode. The Raman signal of Si disappeared at voltage below 0.1V, indicating formation of Li-Si alloy [33]. The experiment confirms the alloying and dealloying of Li-Si. Also, it indicated that the crystalline Si goes to amorphous phase during discharge-charge process.

To further improve the capacity and cycling behavior of the composite anodes, different

modifications are used. One strategy is to improve the bonding between silicon and carbon. For example, a post thermal treatment at 800℃ in nitrogen atmosphere was carried out to improve the bonding between silicon and carbon nanotubes [34]. X-ray Photoelectron Spectroscopy(XPS) showed that silicon oxides appear after the treatment. The post treatment was quite successful to improve the first cycle efficiency as well as the capacity retention. Calcium modification was carried out on a silicon/carbon composite anode material by adding $CaCO_3$ on the pyrolysis precursor. Compared to the silicon/carbon composite, the silicon/carbon/calcium composite anode showed much better cycling behavior. By XRD study, it was pointed out that trace amounts of $CaSi_2$ and Ca_2Si could be produced during pyrolyzing [35], which might have increased the affinity between silicon and carbon. A different strategy was to limit the lithium insertion. In doing so, the cycling behavior of the anode could be increased [36].

The main complication of the mixing method is that with longer grinding time, the irreversible capacity increases due to increased surface area, with weaker attachment of Si to the matrix. However, with extended milling time, the composite will achieve better dispersion, leading to better cycling behavior. It is crucial to acheive a balanced point in the mixture method.

2.5.2 Carbon coated Silicon

Instead of aiming to disperse silicon particles uniformly in a carbon matrix, another type of silicon-carbon method utilizes carbon mainly on the outside of silicon to restrain the volume expansion of silicon upon lithium intercalation, helping to retain the integrity of the anode structure. The carbon coating maintains a conductive network even with a large volume change of silicon. Also, the coating acts as a passive layer for silicon against side reaction with electrolyte. Usually, the preparation of the carbon coated silicon composite involves multiple steps. The anodes produced in this manner showed overall better properties than those using the previously mentioned mixed method.

Pyrolysis is commonly applied in fabrication of the carbon coated silicon composites. It is usually done through decomposition of carbon precursor wrapping the surface of silicon. The pyrolyzing temperature is a key factor in the process. In one case, amorphous carbon coated silicon nanocomposites were made through spray-pyrolyzing a mixture of nanosized Si and citric acid/ethanol solution. Under the optimized pyrolyzing temperature of 400 ℃, the battery with the as-made composites anode showed a good capacity retention of about 1100mAh/g over 100 cycles, which was mainly due to the volume expansion restrain of the amorphous carbon coating [37].

Not limited to silicon particles, silicon nanowires (SiNW) were also incorporated into this kind of composite with pyrolized carbon coating. It was found that control of the porosity and wire diameter is crucial to the properties [38]. The performance was dependent not only on the coherence of the Si/C structure but also the high extent of alignment of the

wires. Carbon aerogel was pyrolyzed and coated on to silicon nanowires into anode as shown in Figure 2.11. The anode showed a good first discharge capacity of 3344mAh/g and Coulombic efficiency of 84%, which was attributed to the conductive and buffer function of the carbon coating [39]. However, the capacity dropped to 1326mAh/g after 40 cycles. From the SEM and TEM pictures, the carbon/silicon interface needed further investigation to achieve better coherence.

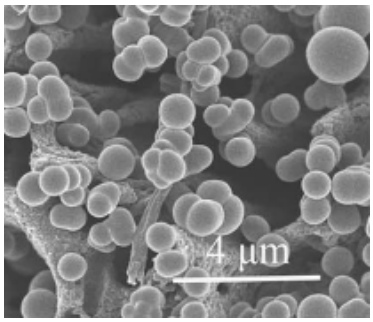

Figure 2.11 Carbon coated silicon nanowires [39].

Chemical and physical deposition methods are also utilized in the carbon coated silicon composites. A silicon/carbon nanotubes core-shell anode material was made by CVD growth of carbon nanotubes on deposited Ni particles on silicon particle surface. The SEM images of the as prepared material indicated that carbon nanotubes covered the surface of the silicon particles and created a cage-like buffer layer [40]. In another case, after plasma enhanced CVD deposition of silicon on copper foil, amorphous carbon film with a thickness of about 100nm was deposited from fullerene C_{60} target to the Si by radio frequency magnetron sputtering [41]. The carbon coating gave the rough bare silicon a much smoother surface and lower electronic resistance. UV/vis results indicated

the deposited carbon film has semiconducting properties. Compared with bare silicon, the composite anodes showed much better cycling stability.

To further improve the properties of the carbon coated silicon anodes, researchers have turned to advanced types of polymerization for better coating and stronger combination of silicon and carbon. A Resorcinol-formaldehyde (RF) microemulsion polymerization with hydrophobized Si nano-particles and post carbonization was studied [42]. Another group fabricated carbon coated Si nanocomposites by ultrasonic-assisted in situ polymerization of Poly (cyclotriphosphazene-4, 40-sulfonyldiphenol) (PZS). Compared with the traditional mixing-pyrolyzing prepared anode, the advanced anode proved to have more uniform dispersion of nanoparticles and better electrochemical behavior. The anode exhibited a capacity of 1200mAh/g after the 40th cycle [43], which was attributed to porosity of the material and the uniformity of carbon coating.

The carbon coated silicon composites were fully characterized. In one study of the pyrolyzed composite, Differential Scanning Calorimetry (DSC) test results indicated the carbon-coated Si anode material had better thermal stability than graphite [44]. The capacity fading mechanism of the anode material was studied by ex situ X-ray and impedance spectra investigation [45]. It was pointed out that more and more lithium ions were trapped in the alloy without extraction, resulting in dramatically decreased in Coulombic efficiency. The crystallinity of silicon also kept decreasing during cycling, which was suppressed to some extent by the carbon coating.

2.5.3 Carbon Silicon Core-shell structure

One more recent category of silicon-carbon anode composite is carbon-silicon core-shell structure. Instead of depositing carbon on surface of silicon, silicon is deposited onto the carbon surface. The silicon is buffered by the carbon structure underneath. By optimizing the carbon structure, the volume expansion of silicon can be compensated. The advantage over carbon coated silicon structure is that the electrical conductivity of the anode is maintained through direct contact of carbon to the current collector. This kind of structure often includes the use of chemical vapor deposition or sputtering. To obtain an anode material with good cycling performance, the coated silicon layer needs to be uniform and continuous.

The parameters that affect the state of deposited silicon include temperature, flow rate, pressure and time. It was found that low pressure, slow flow rate and low temperature would assist the penetration of precursor gas into the array [46]. Amorphous silicon is preferred in terms of stable cycling behaviour. In a microwave assisted CVD process at 900℃, Raman spectroscopy showed the coating consisted of mixture of amorphous and crystalline silicon. The coating composition was dependent on time, where shorter coating time gave more amorphous silicon [47]. The cycling test showed a trade-off in the increase in capacity and the decrease in electrical conductivity.

Another group made a hybrid silicon–carbon nanostructured composite using a conventional sputtering system [48]. The sputtered amorphous silicon seemed quite

uniform in the SEM image of the as-made composites. The optimization of silicon thickness considering capacity is shown in Figure 2.12. The structure did not have high enough integrity as core-shell composites. The advantage of the method mainly relies on the amorphous nature of the sputtered silicon. If we can combine the structure and the amorphous silicon together, the properties could be further improved.

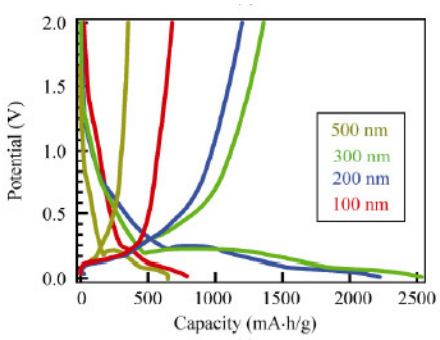

Figure 2.12 Voltage profile of silicon-carbon anodes [48].

A uniform silicon coating can be achieved by simulating atomic layer deposition through periodically feeding of reactant gas and a controlled growth mechanism. Silane gas was pumped into a reactor chamber at 30℃ around 500 Pa for adequate penetration [49]. Then temperature and pressure were raised for Si deposition reaction. The above mode was repeated for several cycles before deposition was stopped. TEM images in Figure 2.13 showed that multi-walled carbon nanotubes were covered with a relatively uniform, continuous silicon layer, which might be due to that the penetration of gas made every particle surrounded with homogeneous reactive atmosphere.

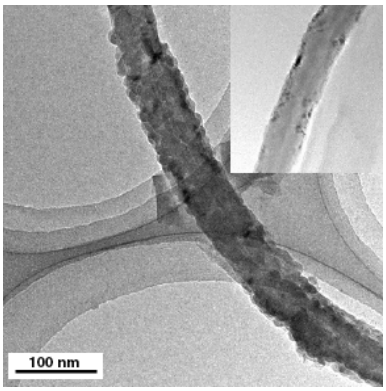

Figure 2.13 Silicon coated MWCNT versus pristine MWCNT [49].

Recently, Wang et al. reported for the first time a heterostructure comprising vertically aligned multi-walled carbon nanotubes containing nanoscale amorphous/ nanocrystalline Si using a two-step liquid injection CVD process. The heterostructure exhibited a high capacity of about 2050 mAh/g [50]. In the structure, EELS spectra revealed that there was an interfacial amorphous carbon layer anchoring the nanoscale Si droplets to carbon nanotubes. However, the extraordinary structure of vertically aligned carbon nanotubes was not utilized. During battery assembly, the as prepared material was incorporated into a slurry with binder and additives. Utilizing the structure of vertically aligned carbon nanotubes which has the potential for the battery to be current collector and binder free, a hierarchical structure from the same group has been made by directly grown carbon nanotubes on Inconel metal foil [51]. Figure 2.14 shows the vertically aligned carbon nanotubes on Inconel foil.

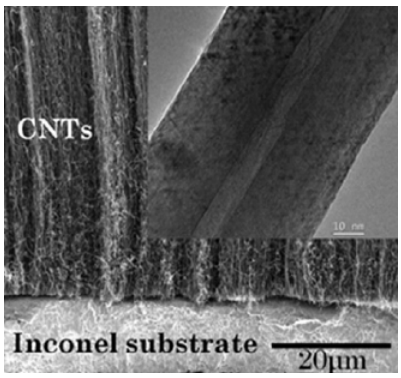

Figure 2.14 SEM image of CNTs grown directly on Inconel substrate [51].

Silicon was then deposited on the as-grown carbon nanotubes as clusters with spacing to each other as seen in Figure 2.15. They utilized the structure of vertically aligned carbon nanotubes as lithium pathway and conducting material. If the silicon clusters could be smaller and more uniform, the property of the anode would be improved a lot. The next step will be eliminating the use of current collector and to control the morphology of deposited silicon.

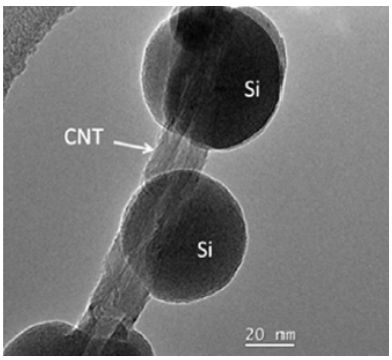

Figure 2.15 HR-TEM image of silicon particles on CNT [51].

2.5.4 Other structures

In addition to the three categories listed above, other novel silicon-carbon composite structures have also been explored. Those trials are far more complex, but reveal valuable information about the design of the composite structure as well.

Scaffold structures were made through pyrolysis of Si-PVdF precursor as shown in Figure 2.16. After pyrolysis, the carbon presented a close-knit structure to hold the Si particles in the net [52]. Electrochemical impedance spectroscopy [53] indicated that the composite had lower charge transfer resistance through cycling compared with bare Si on current collector, which improved the capacity stability.

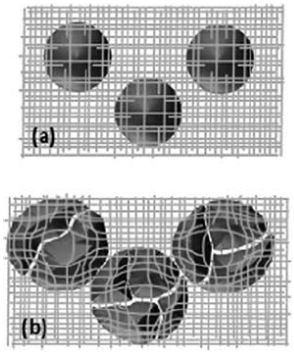

Figure 2.16 Scaffold structure(a) before lithiation(b) after lithiation [52].

Diamond-like carbon was coated on to Si film in different morphologies. The coating was patterned to partially cover the silicon film. Compared with the silicon film anodes fully covered with diamond-like carbon, the partially coated ones showed better cycling properties and reversible capacity [54]. Figure 2.17 presents a SEM image of

diamond-like carbon on top of a silicon film.

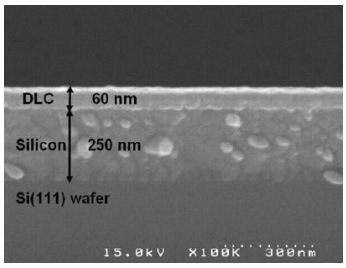

Figure 2.17 Diamond-like carbon on top of silicon film [54].

It is also proposed that materials with volume expansion between aluminum and Si can be added inbetween to further eliminate the difference in strain gradient to achieve a more coherent structure. A three layer composite (Figure 2.18) was made with carbon nanorods coated with aluminum and silicon "nanoscoop" on top by sputtering [55]. Since the strain of aluminum lies between carbon and silicon, it acted as a gradient layer for reducing interface mismatch between different materials, especially for high rate applications which would introduce dramatic strain all through the structure.

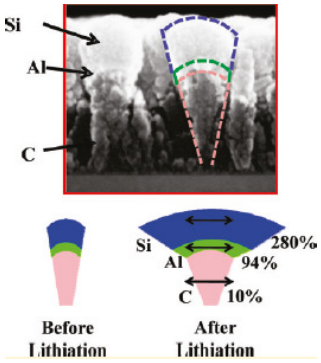

Figure 2.18 Carbon nanorod, aluminum and silicon "nanoscoop" composite [55].

2.6 Challenges and opportunities

There are challenges as well as opportunities in the research regarding silicon-carbon composite anode for lithium ion battery. One challenge is to improve the cycling behavior of anode while reducing irreversible capacity. The former lies in providing sufficient buffer and conductivity all through cycling using carbon material while aiming to maximize the silicon contribution in the composite. The latter depends on reducing the formation of SEI layer on surface of silicon and the amount of trapped lithium ions [56].

Another challenge is to control the phase of silicon. 500 ℃ as an optimized silicon deposition temperature was reported in many studies. However, the phases of the deposited silicon using the optimized condition were different. The phases can be crystalline [57], amorphous [58] and complex mix. In one case, silicon was deposited on bamboo-like carbon nanotubes using Radio frequency sputtering method [59]. The phase of the material was complex; silicon, silicon carbide, silicon oxides were all present in the sample. The varied phases of silicon may relate to the different carbon materials. However, the combination of temperature, pressure and flow can have major effects on determination of the nature of deposited silicon.

An exciting opportunity is the possibility to increase the energy density dramatically once the anode is current collector and binder free. The current collector weighs much more than active materials in batteries in experiments. The binders and additives lower the mass fraction of active material significantly as well. In one study, silicon was deposited onto stainless mesh supported CNT network to obtain a current collector free anode [60]. The energy density was increased by ten times compared to an anode with Cu collector. Once all the inactive weight of anode part is removed, the energy density can be further improved.

3. Experimental

3.1 Material preparation

3.1.1 Carbon nanotube array growth mechanism in CVD system

Although a lot of research has covered the topic of carbon nanotube growth, the exact mechanism of the growth is hard to determine for a particular growth process. Different growth conditions can also present different growth mechanisms. The most popular CNT growth mechanism theory assumes each carbon nanotube grows with a catalyst particle on top. The precursor gas decomposes under the catalyst particle to support the growth of the tube. The growth of the tubes in CNT arrays can either be extrusion (base-growth) or tip-growth as shown in Figure 3.1. In the extrusion theory, carbon nanotubes grow with the catalyst particles attached to substrate while the tubes grow on top of the particles. In tip-growth theory, carbon nanotubes grow with the catalyst particle on top [61]. Once the catalyst loses activity, the carbon nanotube growth will stop. If the growth of carbon nanotubes stops while the precursor gas supply continues, there will be amorphous carbon deposited on the tubes, lowering the quality of carbon nanotubes in most cases.

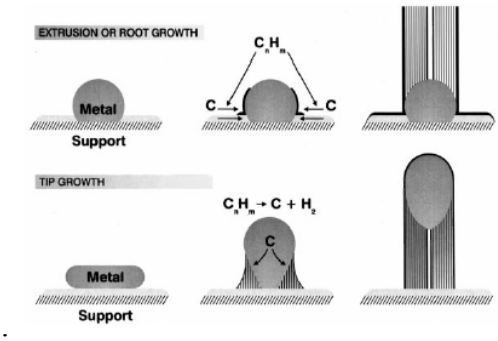

Figure 3.1 Schematic picture of carbon filament growth [61].

3.1.1.1 Construction of low pressure CVD system

A vapor phase catalyst deposition method was used to grow carbon nanotubes. A low pressure chemical vapor deposition system (LPCVD) suitable for this method was custom built as shown in Figure 3.2. The furnace chamber is a quartz tube with a 76 mm diameter. A smaller quartz tube with a length of 74 cm and a diameter of 64 mm is inserted to the outer tube to load substrates. There is a quartz window (shown in Figure 3.3) on the door of the furnace chamber, allowing the inside of the chamber to been seen during the growth run. Compressed gas lines run from the top of the furnace through mass flow controllers and converge into a single main gas line. Gases come down the main gas line into the front of the quartz tube and go through the hot zone, a filter, a pressure controller, and then to a mechanical pump. The carbon nanotube yield of the system is very high. After completing a growth run, all of the substrates and tube within the hot zone (about 25 cm in length) were covered by carbon nanotubes.

Figure 3.2 Low pressure chemical vapor deposition system.

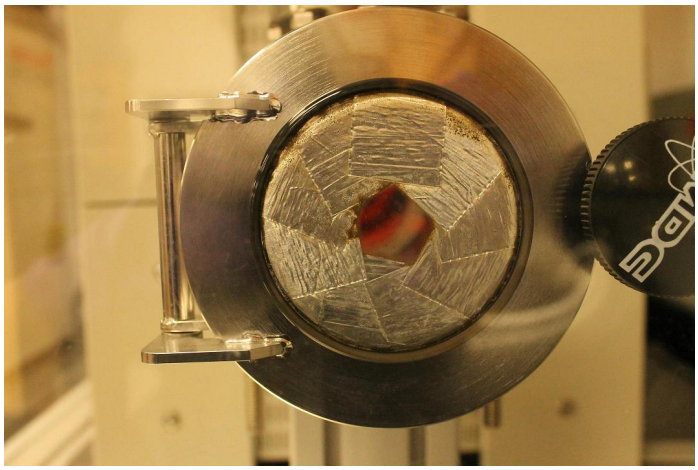

Figure 3.3 Quartz window on chamber door.

3.1.1.2 Optimization of carbon nanotube growth parameters

Square quartz substrates with dimensions of 25 mm x 25 mm were first burned at 800 ℃ in air for 5 minutes to remove any carbon based residue on the surface of the substrates. After the heat treatment the substrates were etched in a hydrofluoric acid bath (less than 0.05% percent concentration) for 1.5h to produce a pristine layer of quartz for the CNT growth process. After removal from the acid bath, the substrates were rinsed with de-ionized water and dried.

The inner tube was also burned and etched in the hydrofluoric acid bath for 1.5 hours before each run. Catalyst iron chloride ($FeCl_2$) powder was weighed out using a balance and placed in a ceramic boat under the quartz stage. Then the substrates were placed on the quartz stage in the inner tube, in the center of the furnace hot zone as shown in Figure 3.4. The system was then closed and pumped down to approximately 6 mTorr before each growth run. The final optimized growth conditions were: 30 minutes growth at 5 Torr and

760℃, with 600 sccm acetylene and 400 sccm 0.5% chlorine in argon. When the chamber is heating up, the catalyst starts to evaporate around 500℃ as seen from the quartz window. The hot zone radiates with a bright orange color starting at approximately 600℃. Before reaching the set temperature, iron chloride is fully evaporated, coating the hot zone with a dark color film. Once the set temperature is reached, acetylene, argon and chlorine gases are released into the system with the automatic control valve regulating the pressure. Carbon nanotubes are nucleated and are allow to grow for the designated time.

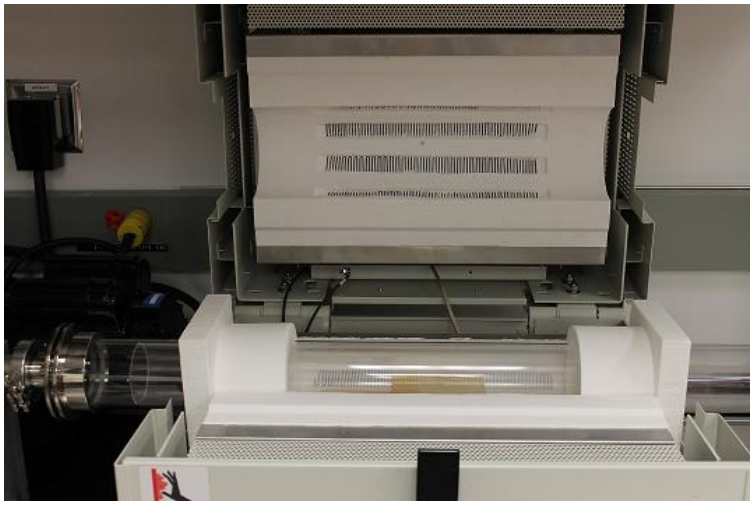

Figure 3.4 Placement of substrates on stage and boat in the furnace.

Temperature, pressure, flow rate, time and the catalyst amount are the key parameters affecting the growth of carbon nanotube array. Optimization of the carbon nanotube array growth was achieved by varying the flow rate of acetylene and catalyst weight. The flow rate was kept low enough to keep the CNT yield high, while being high enough to support long array growth. The catalyst vapor concentration in the hot zone determines the density and diameter of the carbon nanotubes in the arrays. The growth pressure was set

as low as possible to reduce viscous flow effects and to reduce the gas residence time in the hot zone. The Table 3.1 shows the different temperature and chlorine flow rates that were tested to find the optimal conditions for long array growth used for lithium ion battery anode:

Table 3.1 Optimization of carbon nanotube array growth conditions.

C_2H_2 (SCCM)	$FeCl_2$ (g)	Pressure (T)	Temperature (℃)	0.5% Cl_2 (SCCM)	Time (min)	Growth
600	1	4	800	no	30	Middle of the tube has CNTs
600	1	4	780	no	30	Growth zone expanded, short array <1mm
600	1	4	760	no	30	Growth zone covered most of hot zone, short array < 1mm
600	1	4	740	no	30	Growth zone covered most of hot zone, short array < 1mm
600	1	5	760	1000	30	Short array ~1mm covered hot zone
600	1	5	760	400	30	Long array ~2mm covered hot zone
600	1	5	760	100	30	Long array ~1.5mm covered hot zone

There was a distribution of temperatures across the hot zone, due to heat loss at the edges of the furnace. According to the manufacturer, the furnace has a uniform hot zone across a 12 cm section in the middle of the furnace. To achieve relatively uniform growth along

the hot zone, lower temperatures were found to be preferable. When chlorine was added to the growth recipe the carbon nanotubes obtained the highest length per 30 minute growth time of over 2 mm. The function of chlorine was not clearly known. It was assumed that the chlorine cleaned amorphous carbon during growth to extend the life of catalyst.

3.1.2 Si deposition on carbon nanotube arrays

Silane was used to deposit silicon in the same low pressure chemical vapor deposition system described in the previous section. The goal was to evenly and individually coat every CNT in the arrays with silicon. Penetration of the silane gas through the carbon nanotube array was crucial to achieving a uniform coating.

Table 3.2 shows the different conditions used to deposit the silicon. Temperature, pressure and gas flow were key factors in determining the morphology of the coating. Low temperature and flow rate were preferred to help achieve slower decomposition of silane. Low pressure helped silane penetrate the carbon nanotubes within the arrays. Among all three factors, temperature had a dominant effect. There was a minimum temperature threshold that had to be crossed to give significant deposition of silicon. The table also indicated that higher pressure and temperature lead to higher deposition rate while decreasing the uniformity of the coating.

Table 3.2 Optimization of silicon deposition conditions.

Number	0.2%SiH4 (SCCM)	Temperature (℃)	Pressure (T)	Time (h)	Si content (wt%)	Deposition
1	500	550	10	1	41	Heavy brown
2	500	500	10	1	-	Black
3	500	550	10	0.5	22	Brown
4	500	550	20	0.5	21	Brown
5	500	550	5	0.5	-	Black
6	500	550	30	0.5	20	Brown
7	500	525	10	0.5	2	Slight yellow
8	500	575	10	0.5	27	Heavy brown
9	500	550	10	0.5	13	Flow gas heating, slight yellow

Comparing samples #3 and #9 in Table 3.2, the only difference in the deposition condition was the time at which silane was allowed to start flowing into the reactor. Silane flowed into the chamber at the beginning of heating up for sample #9. While for sample #3, silane started to flow right at the set temperature. Sample #9 showed little color change while still obtaining 13% weight percent silicon. However, sample #3 had a heavy brown color on top. This indicated that silicon deposition was more uniform in sample #9. In sample #9, instead of accumulating mostly on top of the array, silicon

penetrated the whole array better. Due to this observation of more uniform silicon deposition, the silane flow was started at the beginning of the heating process, instead of releasing the silane after reaching the set temperature, in all the subsequent silicon deposition experiments.

After the first set of silicon deposition experiments it was found that the quartz tube was permanently coated with silicon and could not be cleaned. Oxidative treatments at high temperatures were attempted to produce silicon dioxide but were unsuccessful. In order to protect the expensive outer tube of the system from silicon deposition, a thick layer of amorphous carbon was coated on the outer tube every time before silicon deposition. The deposition condition for the carbon coating was 1.5h under 760℃, 20 Torr and another 1.5h under 800℃, 20 Torr to ensure that the outer tube was covered entirely as shown in Fig 3.5. Silicon deposited on the amorphous carbon layer instead of the quartz. After silicon deposition the amorphous carbon was burned in air to remove the coating and the tube could then simply be wiped clean.

Figure 3.5 Outer quartz tube with amorphous carbon coating.

Due to the effect of amorphous coating on outer tube, the optimized deposition temperature was increased to about 605 ℃ to 625 ℃， which was higher than the temperatures found in Table 3.2. It was thought that this increase in optimal deposition temperature could be a result of the black amorphous carbon absorbing the infrared radiation normally penetrating the clear quartz tube, changing the temperature at the thermocouple that was outside of the quartz tube. The optimized pressure and flow for silicon deposition remained at 10 Torr and 500 sccm. Control of the deposited silicon weight was realized through altering the deposition time. The weight ratio of silicon was determined by weighing the carbon nanotube arrays and substrate before and after silicon deposition.

Before electrochemical testing was conducted, the deposition uniformity was evaluated through observing the color of the array and substrate. The pristine array was black, as seen in Figure 3.6. When a relatively uniform coating was made, the array turned a light brown color, and the quartz substrate had some silicon deposition, as seen in Figure 3.7 and 3.8. When the temperature was too high, the silicon deposited quickly at the surface of the array. If most of the silicon accumulated on top of the array, the array surface was a solid light-brown color and the substrate was mostly clear, as shown in Figure 3.9 and 3.10.

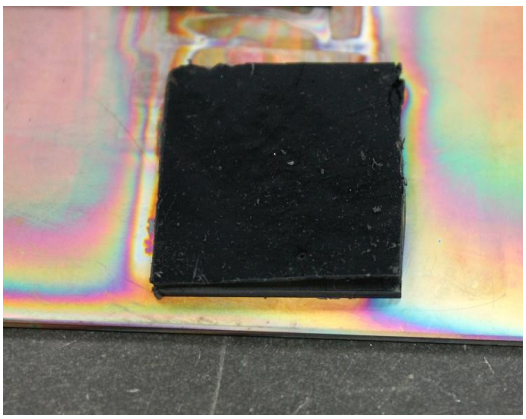

Figure 3.6 Carbon nanotube array before silicon deposition.

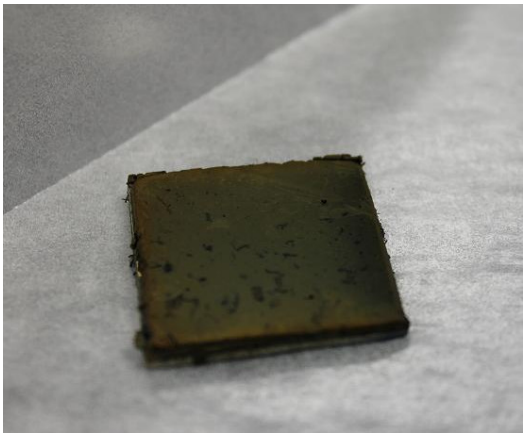

Figure 3.7 Silicon deposition at the optimized conditions.

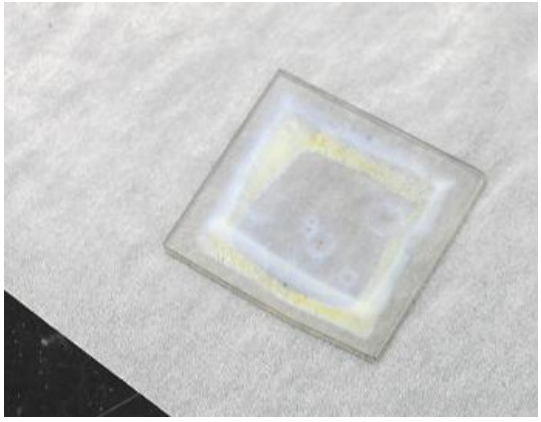

Figure 3.8 Substrate after silicon deposition at the optimized conditions.

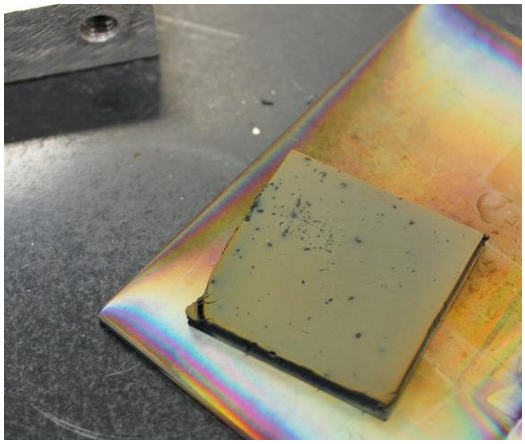

Figure 3.9 Silicon deposition accumulation on top of the array.

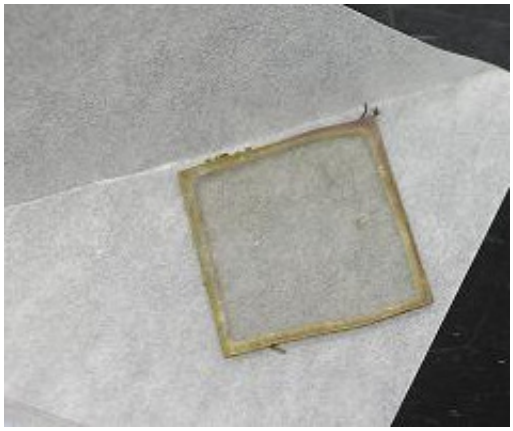

Figure 3.10 Substrate of the array with accumulation of silicon on top.

3.1.3 Shear pressing Si-deposited carbon nanotube arrays for lithium ion battery anode

The battery anode material should be a thin sheet of material. The carbon nanotube arrays used in this study were very tall (up to 2 mm) and very low density. To increase the density and to reduce the thickness, the arrays were pressed on a special “shear pressing” device to transfer the carbon nanotubes from a vertically aligned structure to a densified, horizontally aligned structure. This device is shown in Figures 3.11 and 3.12.

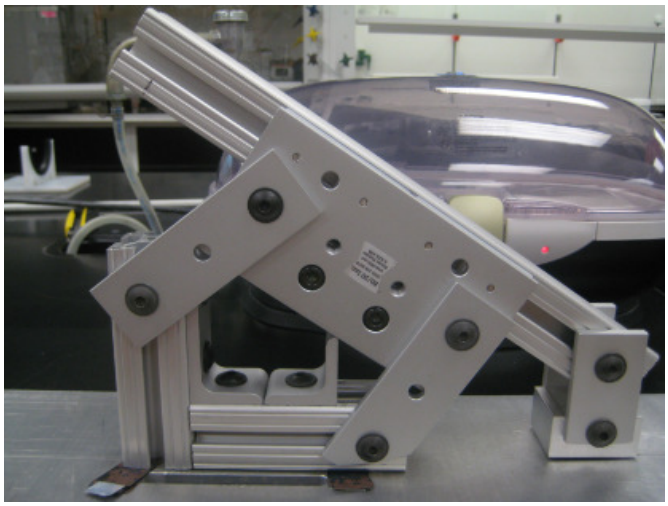

Figure 3.11 Shear pressing machine.

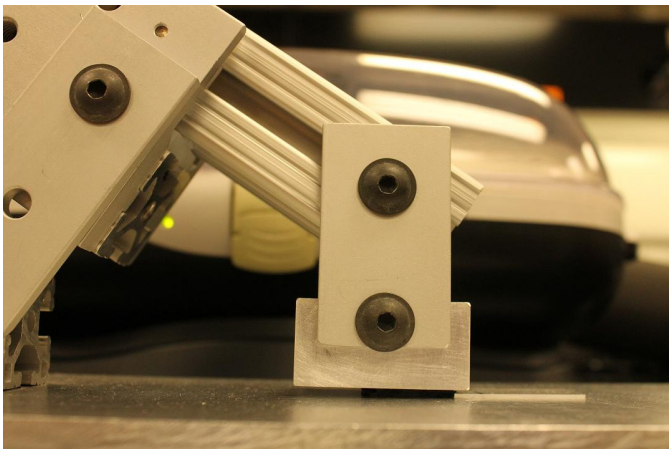

Figure 3.12 Sample shear pressing.

The shear pressing machine consisted of two aluminum parallel plates. One of the plates acted as a fixed base. The other one was fastened to a linear bearing with an adjustable angle [62]. The pressing angle was 34°. Before shear pressing, the composite arrays (on the growth substrate) were placed besides a quartz backstop on the base. Figure 3.13 demonstrates how the morphology of the arrays changes from a vertically aligned structure to a horizontally aligned and densified structure after pressing. After shear pressing, the 1.5 mm tall composite array was changed into a highly aligned film with a

thickness of about 200 μm. The sheet was then easily peeled off from the substrates (Fig 3.14).

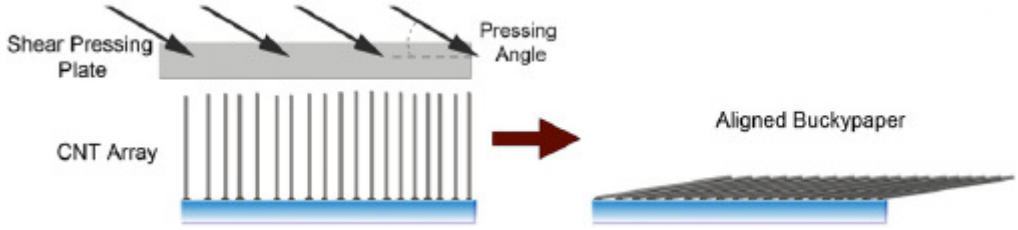

Figure 3.13 A schematic of the morphology of the array before and after shear pressing [62].

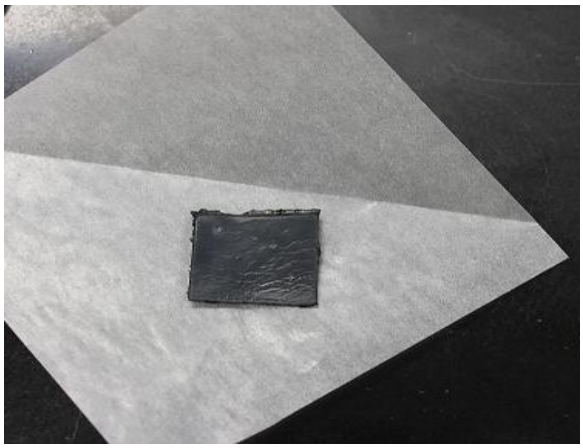

Figure 3.14 Shear pressed sheet.

3.1.4 Cell assembly

The shear pressed silicon-carbon nanotube composite sheet was directly used as anode material without any binder or additives. The sheet was punched into anode piece and assembled into standard 1/2" coin cell battery. Due to the nature of the shear-pressing, materials in the as prepared composite sheet was highly compressed. When the sheet was punched into 1/2" diameter anodes the compression of the battery assembly often resulted

in a short circuit. In order to prevent the short circuit, the anode piece was punched into smaller round pieces that had a diameter of 3/8". Lithium metal foil was used as the counter electrode. The separator used in the battery assembly was monolayer polypropylene (PP). The electrolyte was produce from 1 mole/L $LiPF_6$ in equal ratio of ethylene carbonate, dimethyl carbonate and diethyl carbonate (EC:DMC:DEC =1:1:1) solvent. The coin cell was assembled in an argon glove box. The structure of the cell is shown as following Fig 3.15:

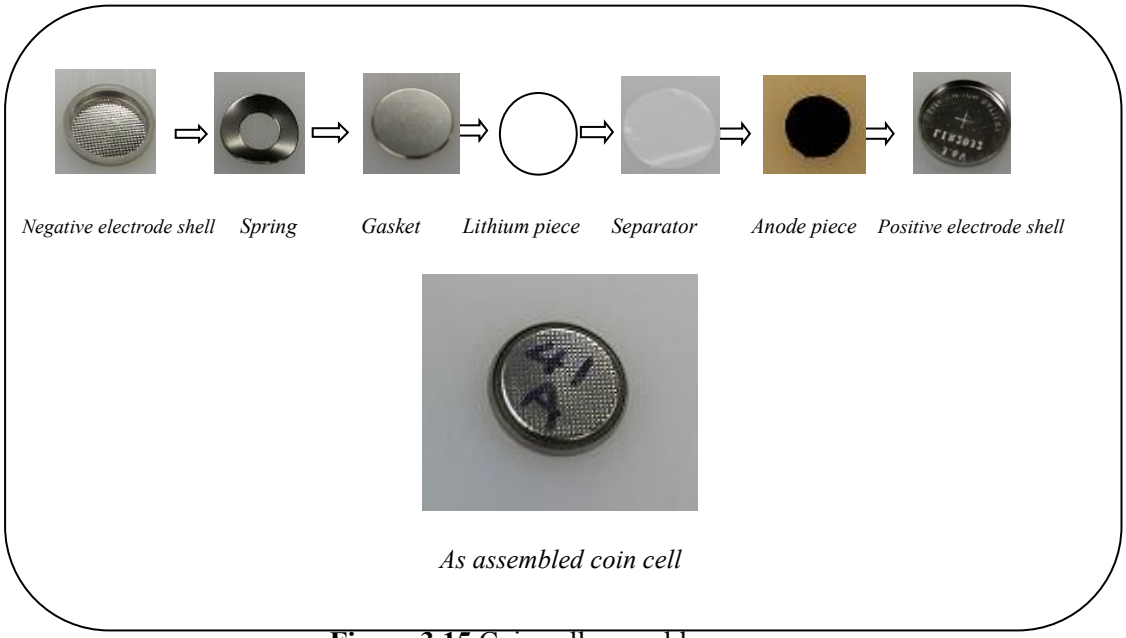

Figure 3.15 Coin cell assembly process.

3.2 Material Characterization

3.2.1Scanning electron microscope (SEM)

The morphology of the as prepared materials was examined using a JEOL 6400 cold field emission SEM. The operation voltage for the samples was 10kV. The samples were attached to grids by conductive carbon tape and directly observed in SEM without

coating.

3.2.2 Transmission electron microscope (TEM)

A Hitachi HF2000 200kV Cold Field Emission TEM was used to observe the CNTs from the arrays and the coating of silicon particles on the CNTs. A small sample of CNTs was removed from an array were dispersed in DI water. The solution was then cast and dried on holey carbon meshed TEM grids for observation.

3.2.3 Elemental Energy-dispersive X-ray spectroscopy (EDS)

To quantitatively analyze the deposition uniformity of silicon in the CNT array, EDS was used to examine the silicon content along the length of the CNTs in the cross section of the array. A Hitachi S3200 variable pressure SEM with a 4Pi Isis EDS unit was applied to quantify the uniformity of the silicon deposition in the array.

3.2.4 X-ray diffraction (XRD)

The crystallinity of the composite material was examined using a Rigku SmartLab XRD machine with a Cu source. The samples were shear pressed thin sheets.

3.2.5 Raman spectroscopy

A Renishaw Raman microscope was utilized to determine the quality of the as grown carbon nanotubes. Also, the effects of post treatment on carbon nanotubes and silicon deposited on carbon nanotube arrays were examined. A 514 nm laser with a spot size of about 10 nm was used to collect data from both sides of the sample sheets.

3.3 Electrochemical characterization

To let the electrolyte fully penetrate the battery system, the coin cells were allowed to sit for 10 hours before tested in a Landit battery test system. They were cycled between 0.1V and 3V with a current density of 50 mAh/g. To insure the repeatability of the test result, as least two data points of the same condition were obtained.

4. Densified carbon nanotube array baseline anodes

4.1 Background

Carbon nanotubes are novel materials whose properties are not studied thoroughly. There are differences between grown carbon nanotubes not only from lab to lab, but also from batch to batch. The insertion of lithium ions are dependent on the structure and defects of the carbon nanotubes. It was necessary to establish a baseline of the shear pressing behavior and electrochemical behavior of the as-grown carbon nanotubes prior to silicon deposition.

4.2 Anode Preparation

Carbon nanotube arrays were grown using the constructed chemical vapor deposition system with the optimized conditions covered in section 3. Various post-treatments were performed to the array to obtain an anode material with stable electrochemical behavior. The post treatments conditions are shown in Table 4.1, including a chlorine post-treatment, carbon post-treatment and thermal post-treatment. The carbon nanotube array anodes were prepared the same way as described in section 3, minus the silicon deposition step.

Table 4.1 Summary of post-treatments conditions.

Post-treatment	Gas flow	Flow rate （SCCM）	Pressure (Torr)	Temperature (℃)	Time (min)
Carbon	C_2H_2	600	5	760	5
Chlorine	Cl_2	400	5	760	15
Thermal	Air	-	Atmospheric	550	5

4.3 Characterization

4.3.1 Physical parameters

The as-grown carbon nanotube arrays were highly aligned 'forest'. The height of the array was approximately 2 mm after 30 minutes growth. The density of the array was approximately 40 mg/cm^3.

4.3.2 Raman Spectroscopy

Raman microscopy was used to examine the quality of produced carbon nanotubes. Also, the effects of different post-treatments on carbon nanotubes were investigated. The following Figures 4.1, 4. 2 and 4.3 are the results from Raman spectroscopy:

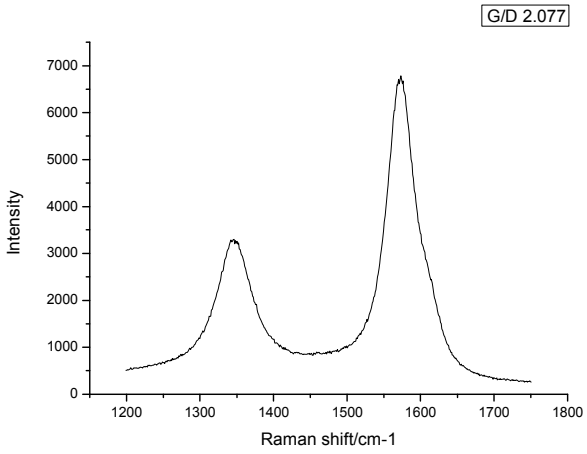

Figure 4.1 Raman spectroscopy of CNT array.

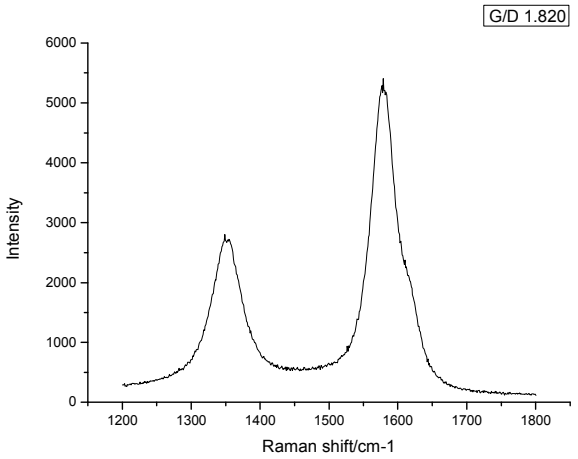

Figure 4.2 Raman spectroscopy of CNT array (carbon+thermal)

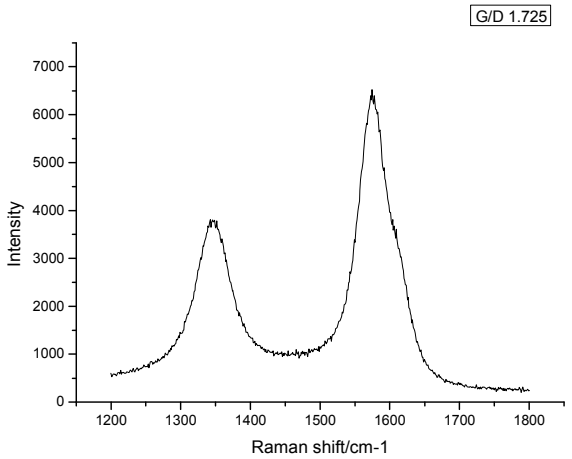

Figure 4.3 Raman spectroscopy of CNT array (chlorine).

The Raman spectroscopy showed the characteristic peaks of carbon nanotubes at 1350 cm^{-1} and 1580 cm^{-1}, which were amorphous (D peak) and graphitic (G peak) carbon respectively. The data plots showed that the G peak to D peak ratio decreased from 2.077 to 1.820 for the array with both carbon and thermal post-treatments. In the chlorine post-treated case, the G to D ratio dropped to 1.725. It was assumed that the carbon post-treatment increased the content of amorphous carbon directly by deposition while the chlorine post-treatment partially damaged the graphene layer of carbon nanotubes. Since the post-treatments introduced more defective sites on carbon nanotubes, it was hypothesized that lithium ion insertion would be promoted.

4.3.3 SEM

Morphology of carbon nanotube array was observed by SEM in Figure 4.4:

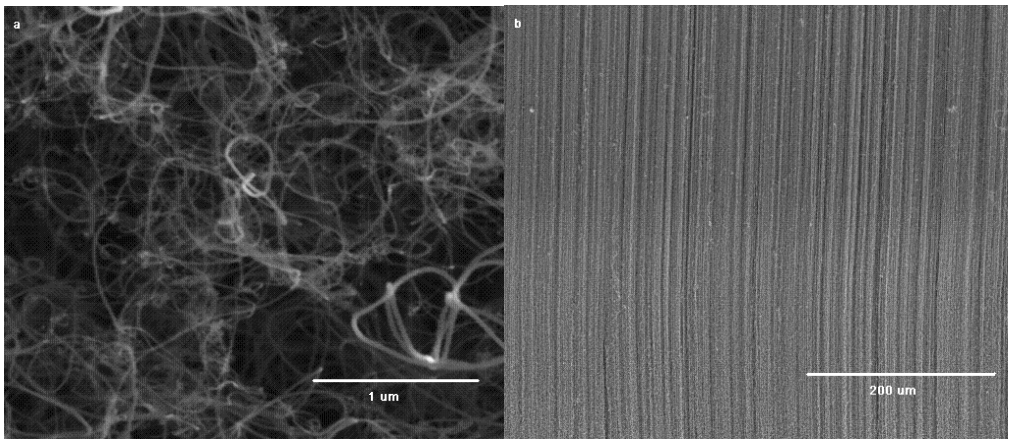

Figure 4.4 SEM image of pristine CNT array a) top of pristine array b) side of pristine array.

The SEM images of pristine carbon nanotube arrays indicated the top of the arrays was like a low density non-woven, with crossed and entangled carbon nanotubes. The array

was a highly aligned vertical CNT structure.

4.3.4 TEM

The internal structure of the as-grown carbon nanotubes was viewed by TEM as shown in Figure 4.5.

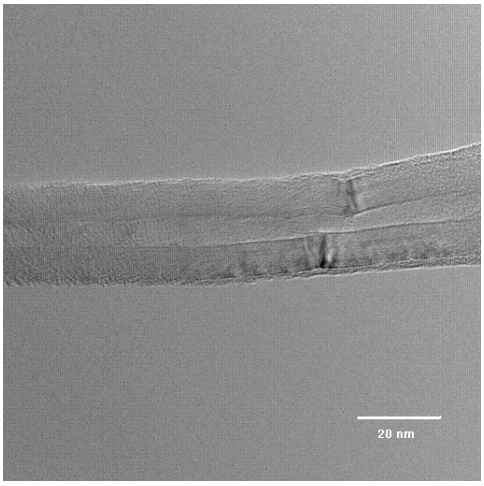

Figure 4.5 TEM image of pristine carbon nanotubes.

TEM images of pristine carbon nanotubes exhibited a hollow core and graphite planes, which revealed the multi-walled nature of the as grown carbon nanotubes. The carbon nanotubes were about 20 nm in diameter with about 20 to 30 walls. The darkened part of the image in middle was assumed to be from the kinks of the tube, most likely formed during the sonication process. The surface of the tubes showed a very thin coating, which was most likely amorphous carbon from the acetylene precursor decomposition on the surface of the tubes during the growth.

4.3.5 XRD

To determine the effect of cycling on the carbon nanotube structure, anode pieces both from before and after battery cycling were subjected to a XRD (Figures 4.6 and 4.7).

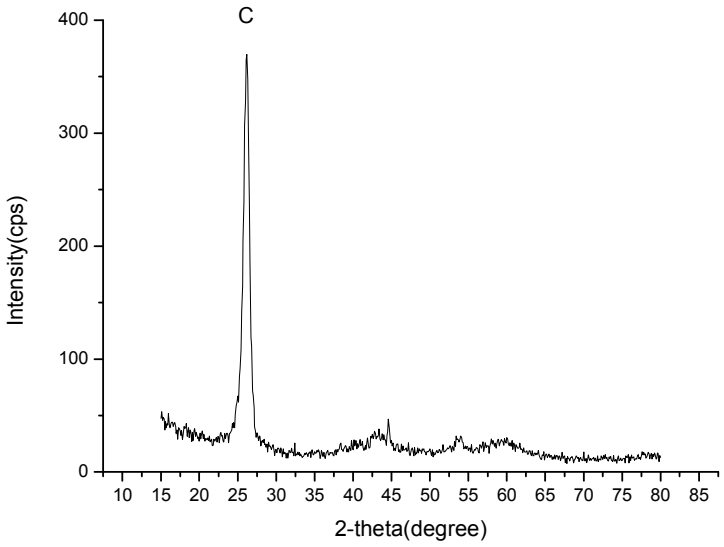

Figure 4.6 XRD pattern of pristine CNT array before cycling.

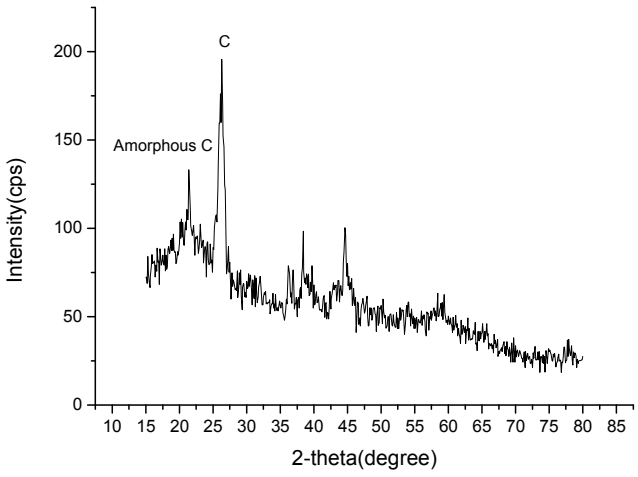

Figure 4.7 XRD pattern of pristine CNT array anode after cycling.

The above results showed that the graphite peak of carbon nanotube array weakened after cycling. A broad peak beside the weakened graphite peak could be observed after cycling, which was likely widened by an increase in defects in the carbon nanotubes during repeated lithium insertion and extraction.

4.3.6 Electrochemical

The cycling behavior for the baseline anodes (as-grown and post-treated) is shown in Figures 4.8-4.12. The green and data points in the cycle number vs. specific capacity graph are the specific discharge and charge capacity respectively. The blue data points show the coulombic efficiency.

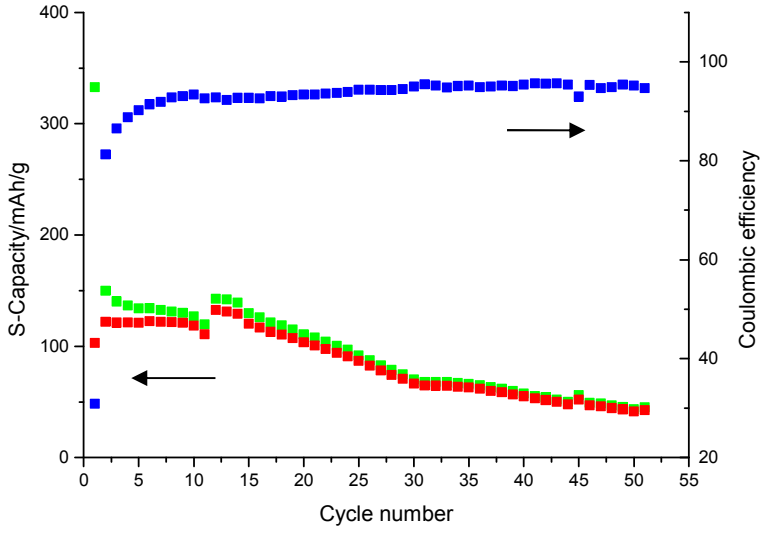

Figure 4.8 Pristine CNT array anode.

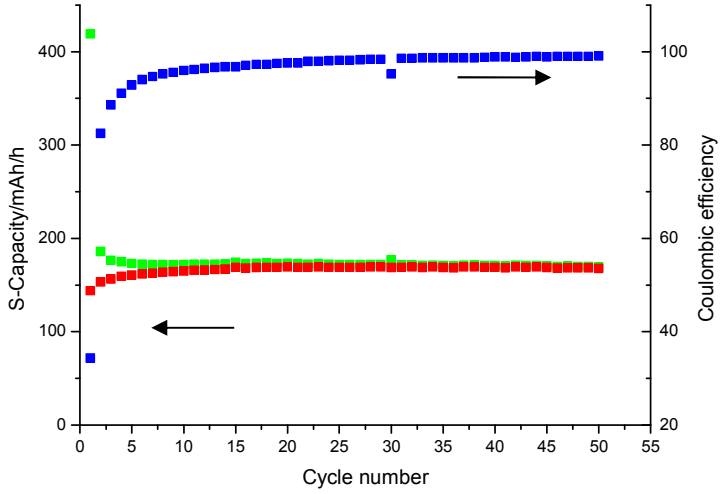

Figure 4.9 CNT array (carbon+thermal) anode.

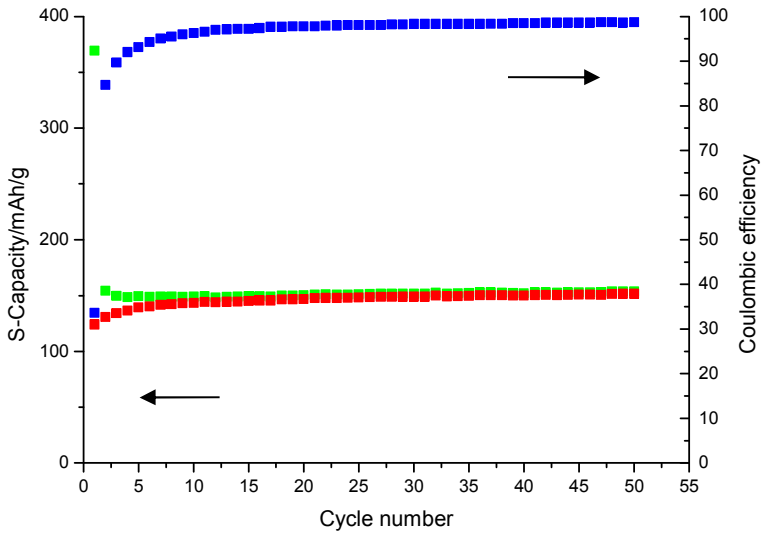

Figure 4.10 CNT array (chlorine) anode.

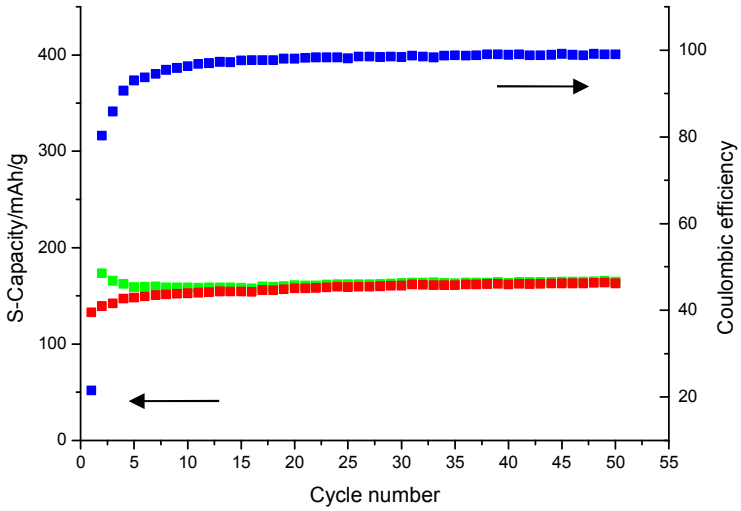

Figure 4.11 CNT array (carbon+thermal+chlorine) anode.

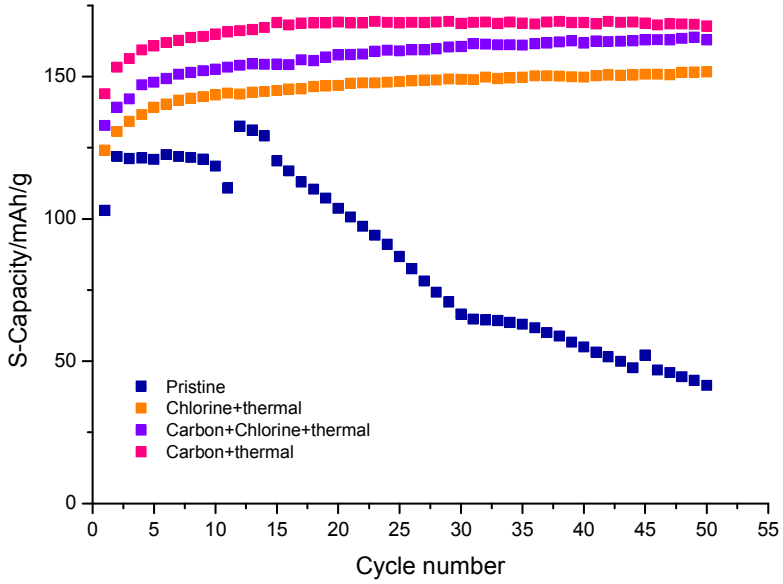

Figure 4.12 Comparison of charge capacities of CNT array anodes.

The comparisons of properties including the initial coulombic efficiency, first cycle charge and capacity retention of the anodes are summarized in Table 4.2.

Table 4.2 Comparison of CNT array anode properties.

	Initial coulombic efficiency (%)	First cycle charge capacity(mAh/g)	Capacity retention at 50th cycle(mAh/g)
Pristine CNT	30.9	102.9	41.5
Carbon+thermal	34.3	143.9	167.7
Chlorine +thermal	33.6	124.1	151.6
Carbon + Chlorine +thermal	21.5	132.8	162.9

The carbon nanotube anodes showed an overall low initial coulombic efficiency. After formation of the SEI layer in the first cycle, coulombic efficiency increased to more than 90% for all the anodes. The post-treated CNT array anodes exhibited higher capacity and better capacity retention than pristine ones. The Raman spectroscopy results showed that the the post-treatments increased the amount of disordered carbon on the carbon nanotubes, which are sites for lithium insertion, which explained the capacity increase. Among the post-treated array anodes, the ones which were carbon and thermal post-treated had the best performance, having a first cycle charge capacity of 143.9mAh/g and capacity of 167.7mAh/g at the 20^{th} cycle. Another interesting observation was that the capacity of post-treated CNT array anodes increased slightly with cycling instead of fading. It is possible that the end cap of the multi-walled carbon nanotubes was removed with repeated lithium ion insertion and extraction [25], allowing for increased lithium insertion.

5. Densified silicon coated carbon nanotube array anodes

5.1 Back ground

Deposition time, pressure, gas flow rate and temperature are important parameters. Fully penetration of Si into carbon nanotube array is a key issue. The Si content in the anode should be controlled to have high capacity while maintain good conductivity.

5.2 Anode preparation

To obtain better bonding between silicon and carbon nanotubes, silicon was deposited on both pristine and post-treated arrays using the same CVD system. After deposition, silicon-CNT anodes were made through shear-pressing and punching. Coin cells were assembled using the procedure outlined in section 3.

5.3 Characterization

5.3.1 Raman spectroscopy

To explore the nature of the as-deposited silicon, the shear pressed silicon-pristine CNT array with about 23% silicon was examined by Raman spectroscopy. Also, the penetration of silicon deposition was investigated by comparing the difference of silicon intensity on top and back of the sheer pressed film. The results are presented in Figure 5.1

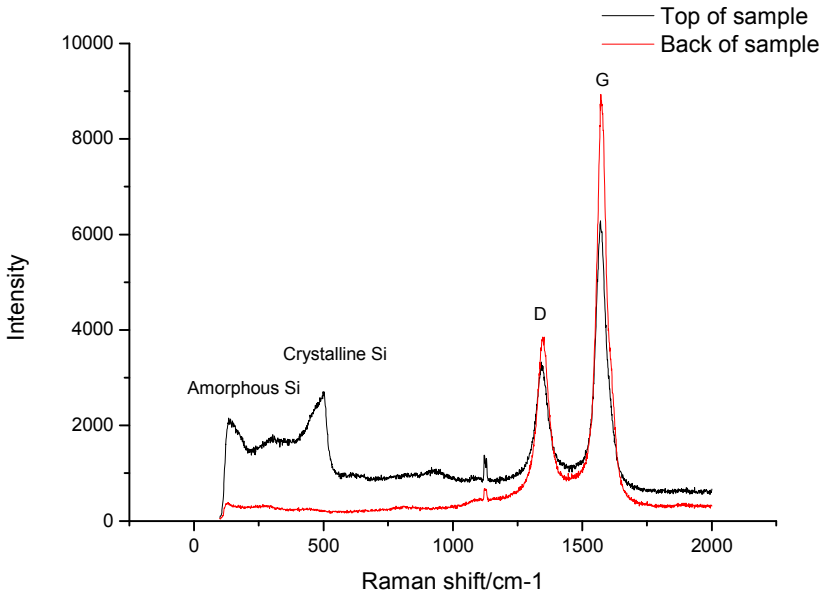

Figure 5.1 Raman spectroscopy on composite CNT array (23% Si) anode.

In the plot, peaks at 1350 cm^{-1} and 1580 cm^{-1} correspond to amorphous and graphitic carbon respectively. Raman results also exhibited strong silicon peaks at around 521 cm^{-1}, indicating the crystalline nature of the deposited silicon on pristine CNT array. The broad peak below 500 cm^{-1} showed the presence of amorphous silicon. The back of the sample showed no significant silicon peak, which means little silicon penetrated to the very bottom of the array for the 1h deposition sample. The result was confirmed by the EDS data.

5.3.2 XRD

The change in silicon structure was explored by comparing XRD data on composite CNT array anode material containing about 23% silicon before and after cycling.

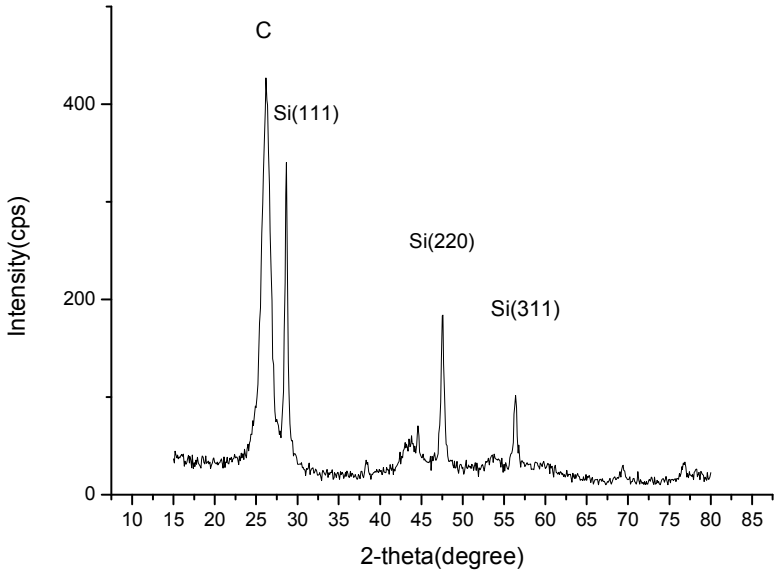

Figure 5.2 XRD pattern of composite CNT array (23% Si) anode before cycling.

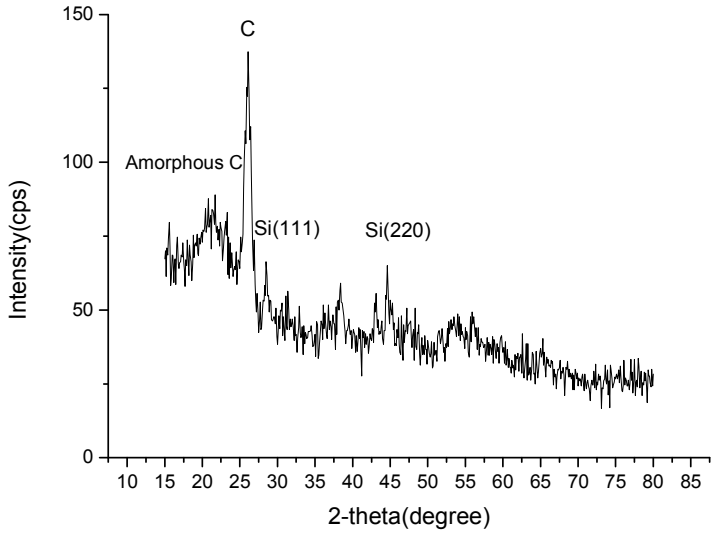

Figure 5.3 XRD pattern of composite CNT array (23% Si) anode after cycling.

XRD pattern in Figures 5.2 and 5.3 indicated that the state of silicon changed after cycling. The peak at 25° corresponded to the (002) layers of graphite [22]. Before cycling, the peaks at 28.4° , 47.3° and 56.1° corresponded to Si (111), Si (220) and Si (311)

respectively [22] After cycling, the silicon peaks weakened and broadened, which indicated the formation of amorphous silicon.

5.3.3 EDS

To investigate the uniformity of silicon deposition more accurately, EDS was used to detect the amount of silicon deposited along the height of the array. Silicon was deposited on pristine arrays under the optimized conditions using different deposition times. During the EDS analysis, three measurements points - top, middle and bottom were taken along a straight line down the array height as shown by the yellow boxes in Figure 5.3. To insure the accuracy of results, various points were measured across the array cross sections. The EDS test results are shown in Tables 5.1 and 5.2.

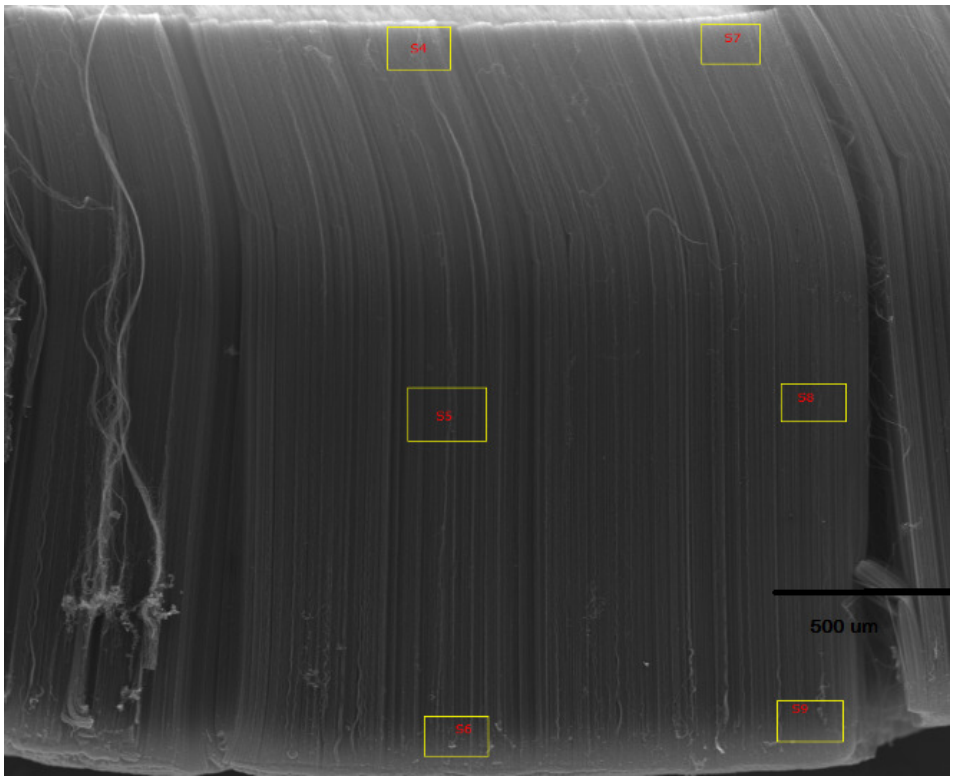

Figure 5.4 VPSEM image of the array for EDS.

Table 5.1 Silicon content from top to bottom of the array with 1h Si (30%) deposition.

Sample / Position	#1 Si content(%)	#2 Si content(%)	#3Si content(%)	Ave.(%)
Top	7.26	8.91	6.71	7.63
Middle	2.54	5.58	2.31	3.48
Bottom	1.3	0.95	0.98	1.08

Table 5.2 Silicon content from top to bottom of the array with 4h Si (54%) deposition.

Position / Sample	#1 Silicon(%)	#2 Silicon(%)	Ave.(%)
Top	43.65	72.05	57.84
Middle	46.16	74.65	60.4
Bottom	56.40	95.91	76.1

For the sample with one hour deposition, the silicon content decreased along the array height, with about 7.63wt% silicon on top and only 1.08wt% on bottom part of array cross section. On the other hand, the CNT array sample with four hour silicon deposition showed relatively uniform silicon content across the array height, ending up with more silicon on bottom than the top. The EDS data indicated that the silicon would first deposit on the top of the array. With increasing time, silicon deposition penetrated the whole array. After almost every single carbon nanotube was coated, silicon started to build up from the bottom. Overall, the data showed that silicon deposition occurred through the whole height of the array even with shorter deposition time.

5.3.4 SEM

To examine the silicon deposition morphology, SEM was used to observe the surface of the shear pressed silicon CNT array anode surfaces. Comparison was made between shear pressed silicon-pristine CNT array anodes with about 23% silicon before and after cycling as shown in Figures 5.5 and 5.6. The SEM sample after cycling was prepared by washing the anode piece with DI water and drying in air overnight.

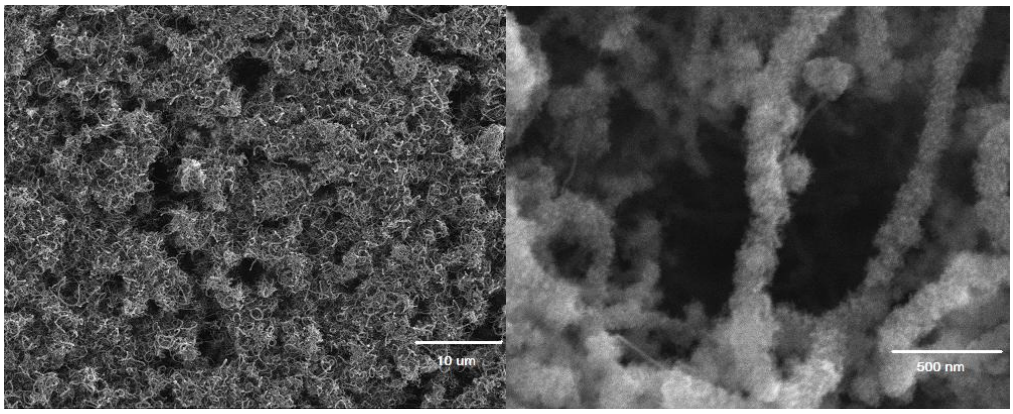

Figure 5.5 Composite CNT (23% Si) anode before cycling.

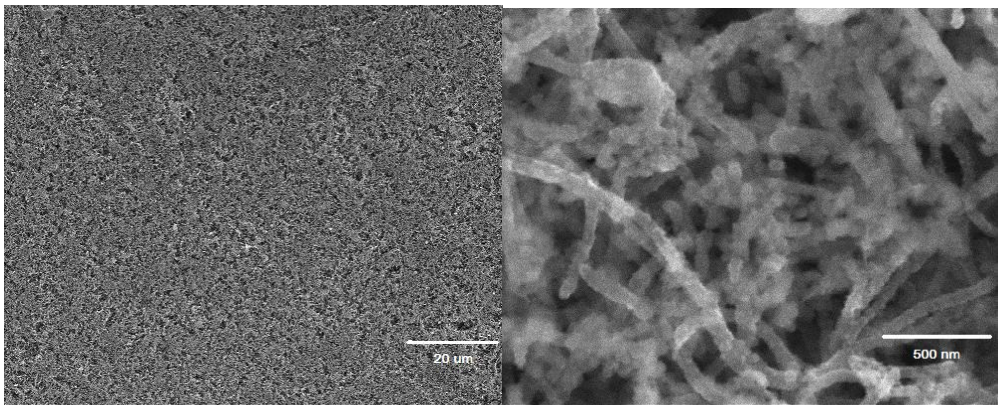

Figure 5.6 Composite CNT array (23% Si) anode after cycling.

The above images indicated that the morphology of composite CNT array anodes before and after cycling showed no significant difference. At lower magnification, the surface of

the anode appeared to remain smooth through the electrochemical process. At higher magnification, the silicon particles stayed on the carbon nanotubes after cycling. The comparison showed that the structure of the anode was quite stable, which is important for the electrochemical performance.

Figure 5.7 and 5.8 show the middle of the array cross section (before pressing), which showed relatively uniform silicon deposition. However, the silicon nano-particles did not attach to each carbon nanotubes very well, with a significant fraction of the silicon distributed in the spacing between tubes. In comparison, silicon deposited on an amorphous carbon post-treated array packed closely to each carbon nanotube. Also, the silicon nano-particles in the pristine array case were much larger in diameter than post-treated ones. It showed that each carbon nanotube in amorphous carbon post-treated arrays were more evenly wrapped with much smaller silicon nano-particles, which was expected to give the anode material better cycling performance. On the contrary, carbon nanotubes in pristine arrays had bigger silicon particles in the space between tubes. In the latter case, carbon nanotubes could not have good contact with silicon, thus losing the buffer function. The difference in the deposited silicon may due to the roughness the amorphous carbon added to the carbon nanotubes surface, resulting more nucleation sites and better bonding.

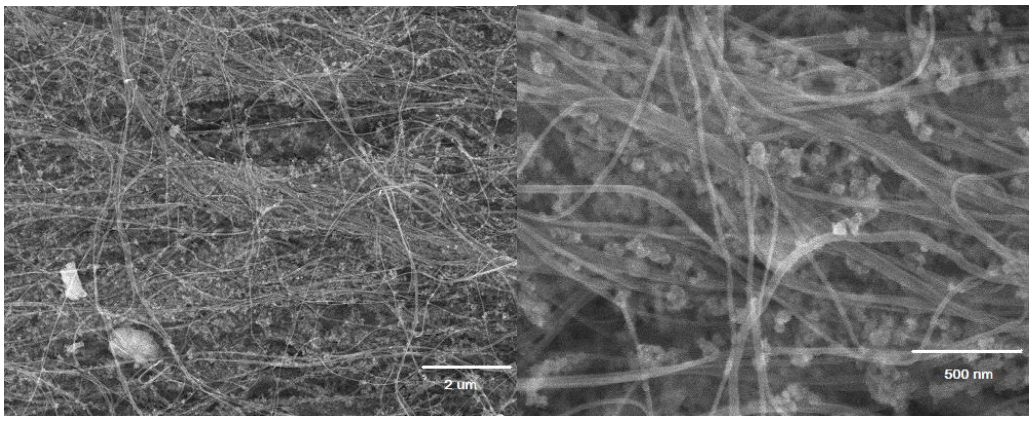

Figure 5.7 Composite CNT array (30% Si).

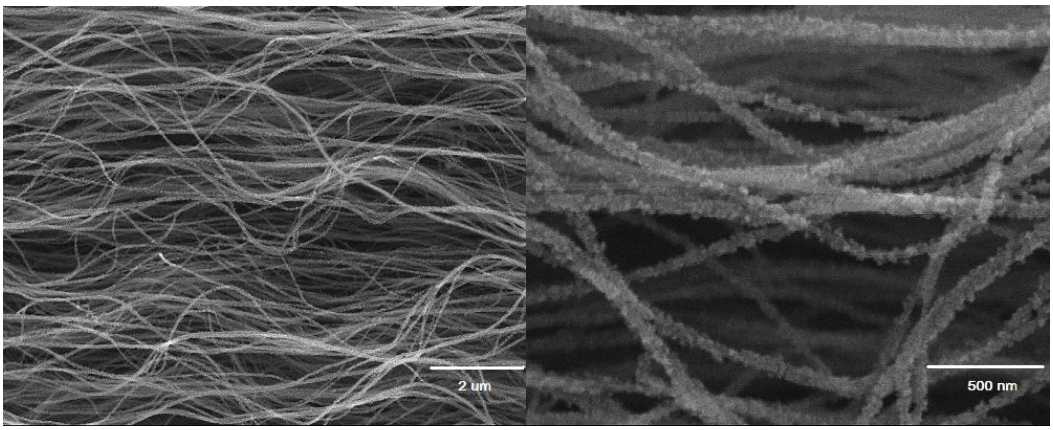

Figure 5.8 Composite CNT array (carbon+thermal+33% Si).

Another thing to notice is that the top of the anode shown in Figure 5.5 indicating good wrapping of silicon particles on tubes for pristine arrays. While the side of the pristine arrays in Figure 5.7 had silicon particles loosely wrapped the arrays and filled in empty space. The difference may indicate that the morphology of the deposited silicon may change through the thickness of the CNT array as well.

5.3.5 TEM

TEM was used to closely observe the structure of the silicon coating on the carbon nanotubes. A carbon nanotube array with silicon deposited on it was dispersed in DI

water and then put into TEM grid.

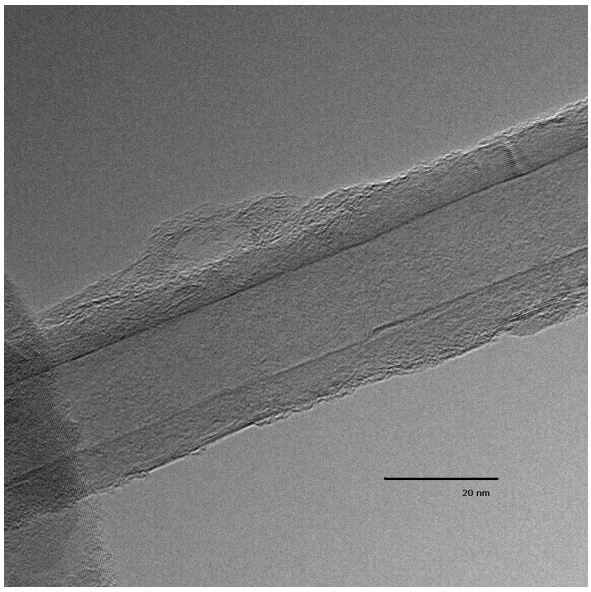

Figure 5.9 TEM image of composite CNT array (30% Si).

In the TEM images Figure 5.9, the graphitic planes of carbon nanotubes were blurry due to the silicon coating. The surface of carbon nanotubes was coated with silicon. The image indicated that silicon on pristine array was nano-particles with a diameter about 20~30 nm.

5.3.6 Electrochemical

5.3.6.1 Cyclic Voltammetry

To explore the potential of the composite, a coin cell with a composite CNT array anode containing 30% silicon was subjected to cyclic voltammetry test.

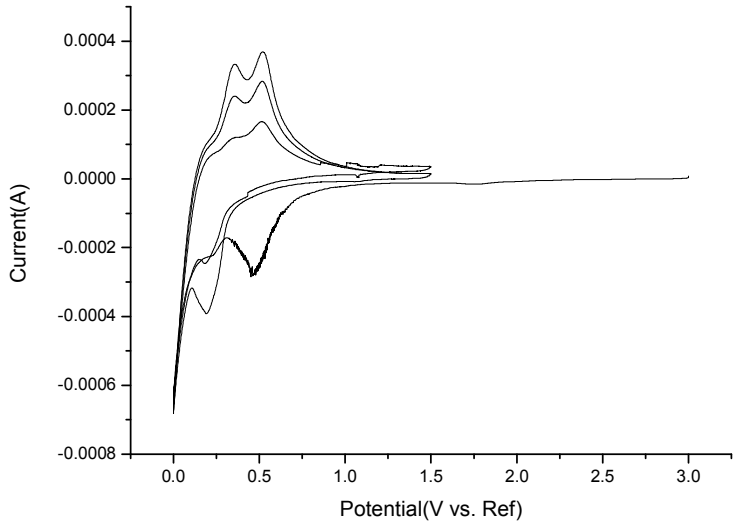

Figure 5.10 CV of composite CNT array (30% Si) anode.

In Figure 5.10, the peaks in the voltage range of 0.5~0.7V may correspond to the formation of SEI layer. The reduction peak at 0.0V and 0.5V in the first cycle indicated the intercalation of lithium ions [56]

5.3.6.2 Cycling tests

Anodes containing different fractions of silicon were cycled on the Landit machine to examine the electrochemical properties of the composites. The silicon was deposited under the optimized conditions in the experimental section -- 605℃~625℃, 10 Torr and 500sccm 0.2% silane balance argon. The silicon content in the composites was controlled by altering the deposition time. The results of the pristine CNT anode with silicon coating are shown in Figures 5.11 through 5.17.

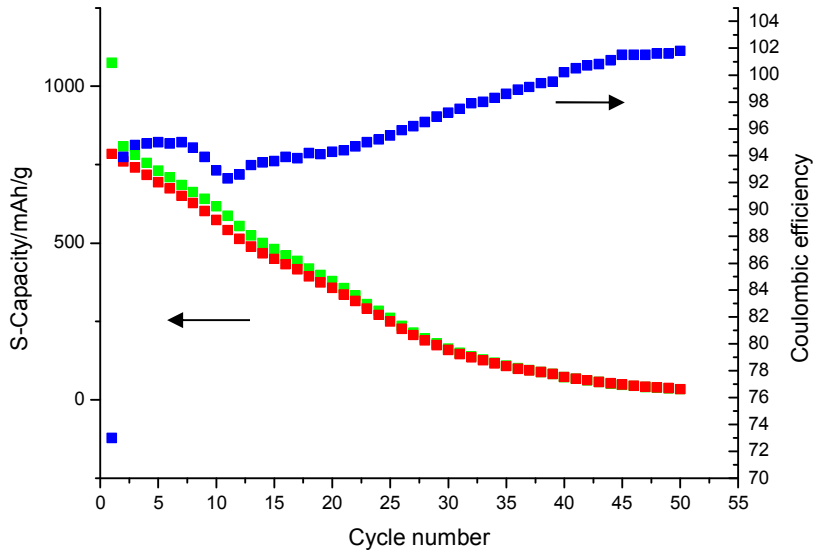

Figure 5.11 Composite CNT array (25% Si) anode.

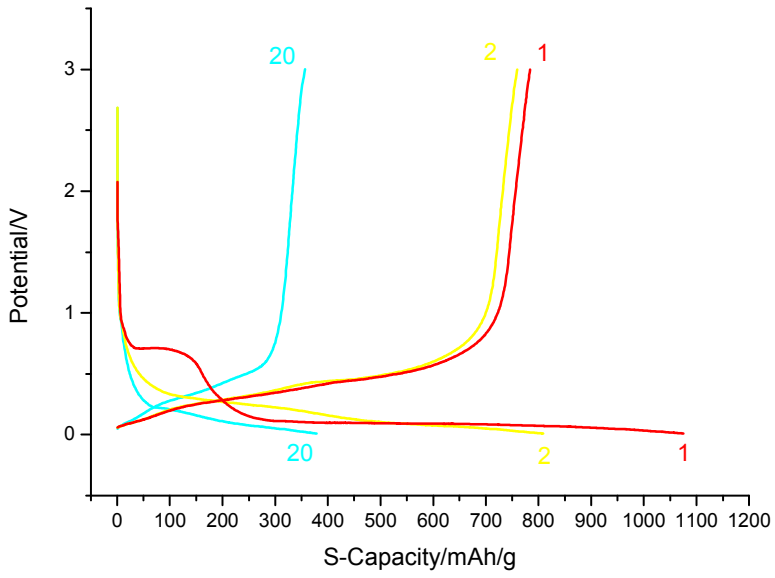

Figure 5.12 Voltage profiles of composite CNT array (25% Si) anode.

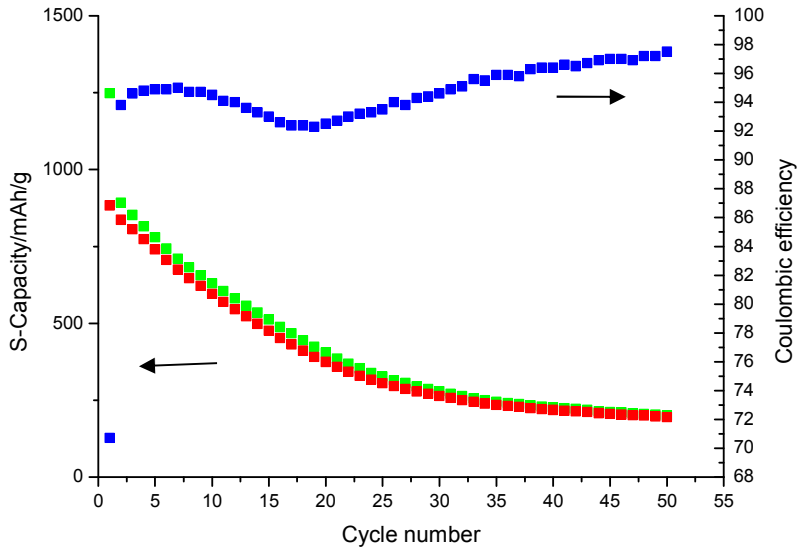

Figure 5.13 Composite CNT array (30% Si) anode.

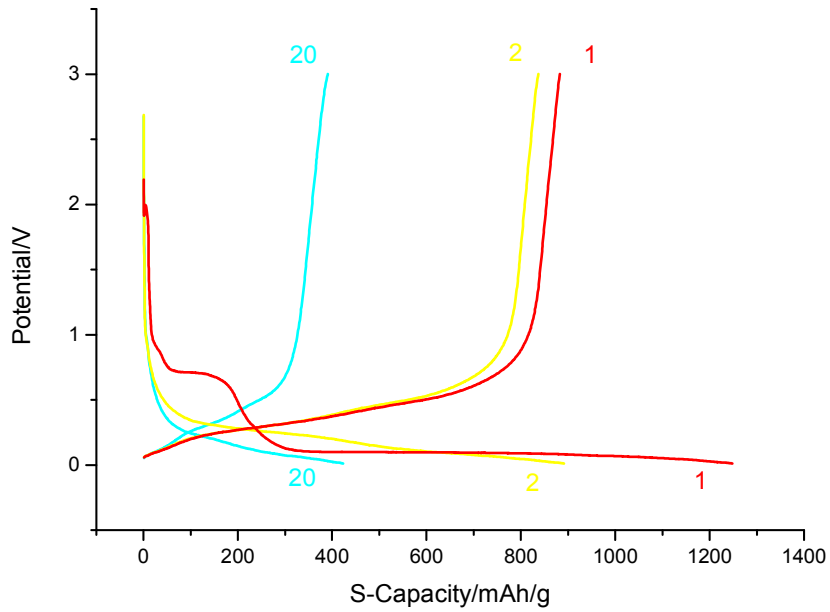

Figure 5.14 Voltage profiles of composite CNT array (30% Si) anode.

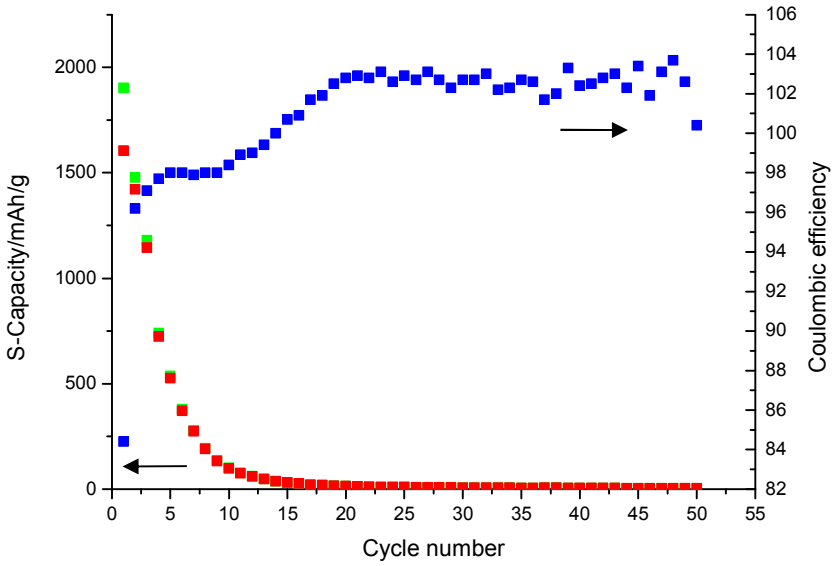

Figure 5.15 Composite CNT array (54% Si) anode.

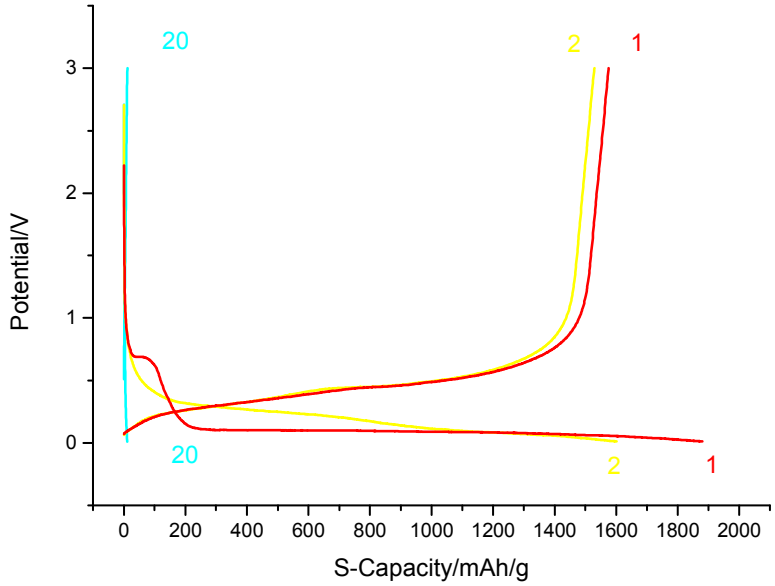

Figure 5.16 Voltage profiles of composite CNT array (54% Si) anode.

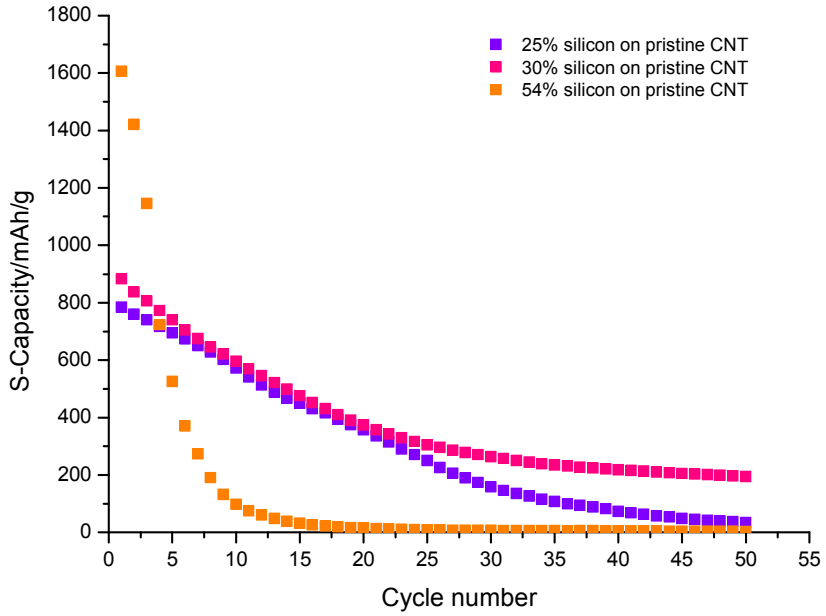

Figure 5.17 Comparison of charge capacities of composite CNT array anodes.

After observing the fast fading of the composite anode, methods were tried to improve the cycling behavior. One way was to deposit silicon on post-treated arrays. In addition, the insertion of lithium ions were limited by reducing the cycling voltage range from 0.01V~3V to 0.01V to 1.5V. The results of the post-treated array anodes containing silicon were shown as below in Figures 5.18 through 5.23:

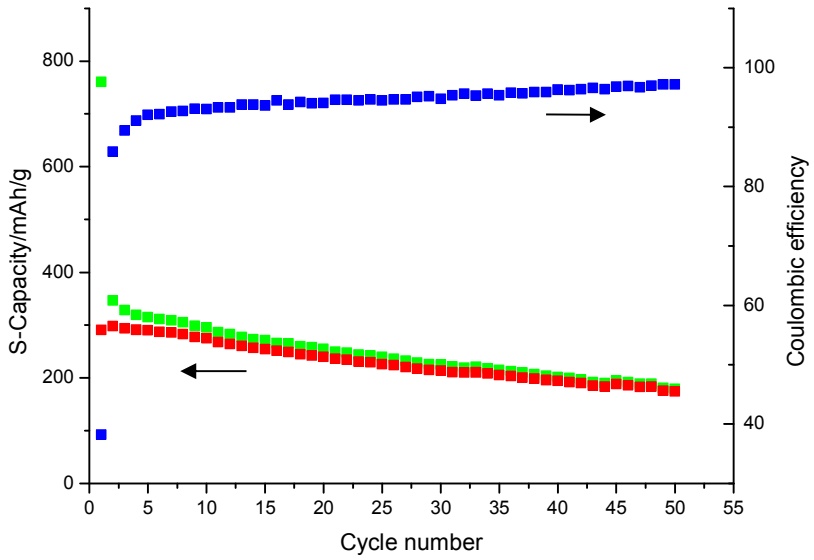

Figure 5.18 Composite CNT array (carbon+thermal+10% Si) anode.

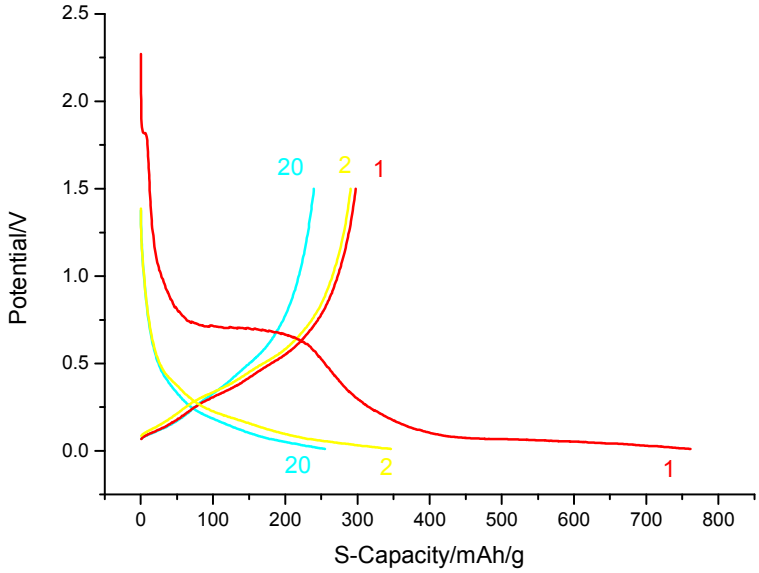

Figure 5.19 Voltage profiles of composite CNT array (carbon+thermal+10% Si) anode.

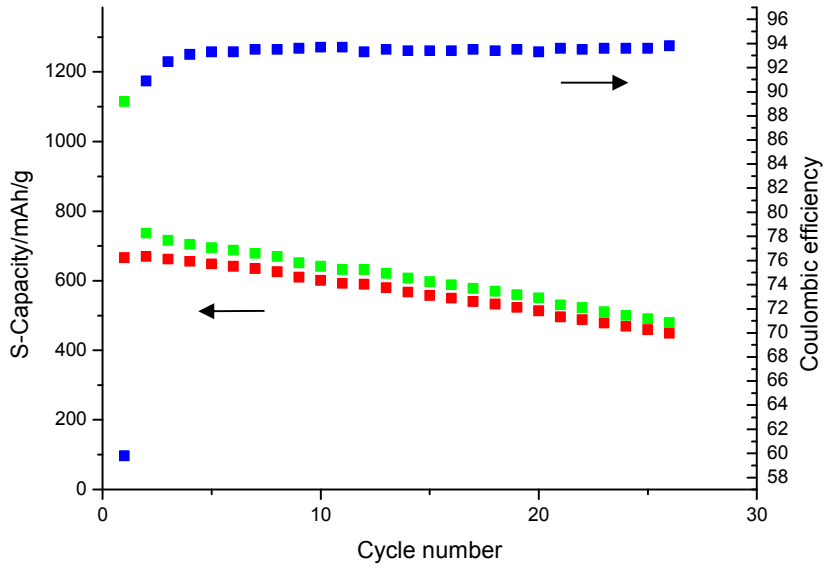

Figure 5.20 Composite CNT array (carbon+thermal+23% Si) anode.

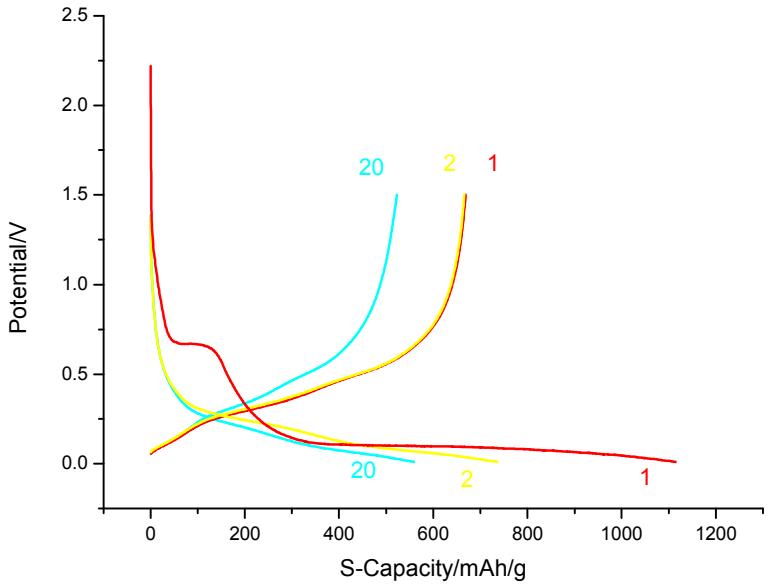

Figure 5.21 Voltage profiles of composite CNT array (carbon+thermal+23% Si) anode.

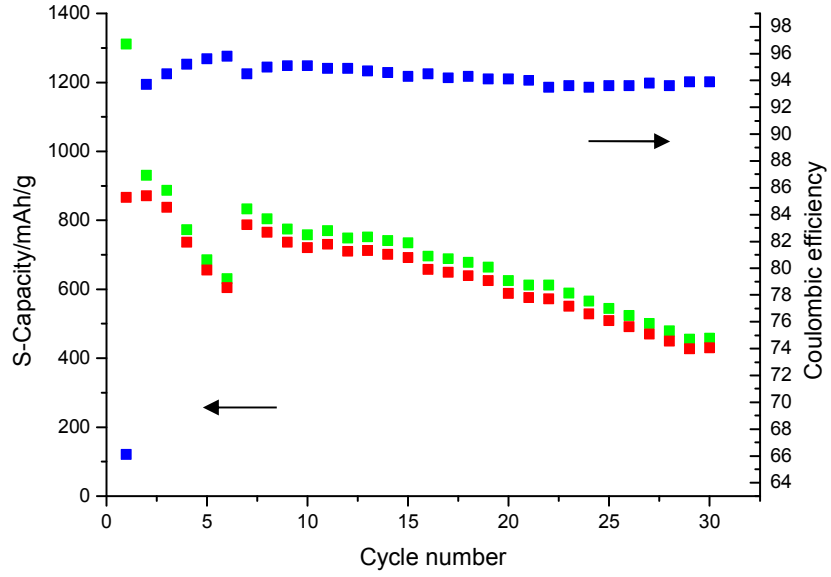

Figure 5.22 Composite CNT array (carbon+thermal+33% Si) anode.

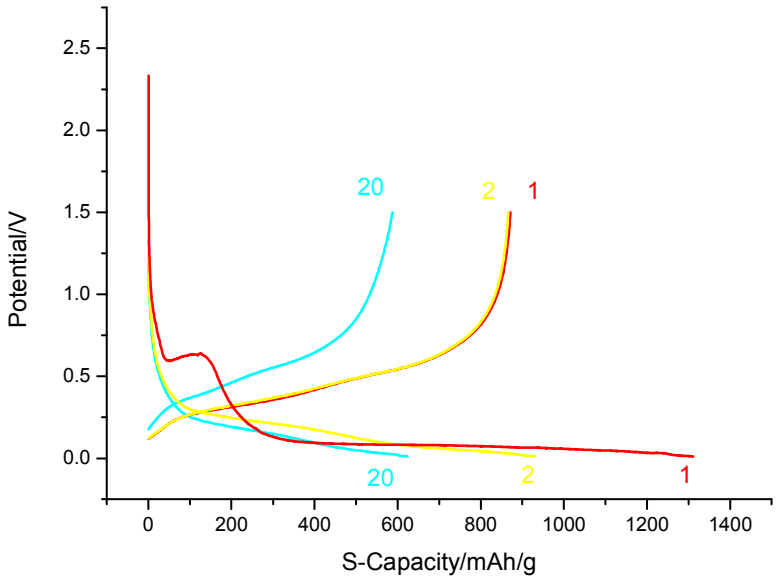

Figure 5.23 Voltage profiles of composite CNT array (carbon+thermal+33% Si) anode.

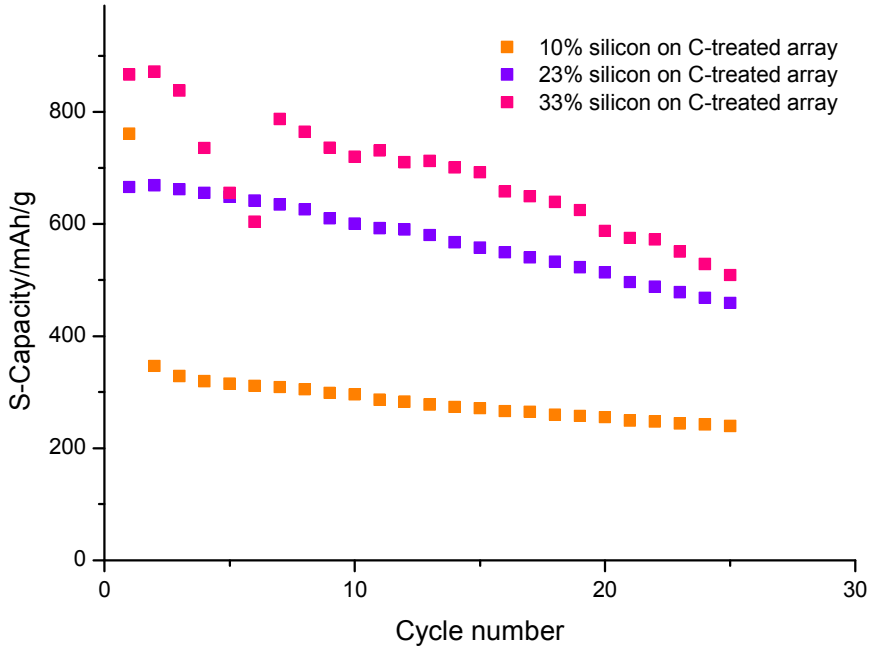

Figure 5.24 Comparison of charge capacities of composite CNT array (carbon+thermal) anodes.

Table 5.3 Comparison of composite CNT anode properties.

	Initial coulombic efficiency(%)	First cycle charge capacity (mAh/g)	Capacity retention at 20th cycle (mAh/g)
Pristine CNT +25%Si	73	784.2	357
Pristine CNT +30%Si	70.7	882.8	373.9
Pristine CNT+ 54%Si	84.4	1606.2	14.2
Carbon post-treatedCNT +10%Si	38.2	290.5	239.8
Carbon post-treatedCNT+23%Si	59.8	666	513.6
Carbon post-treated CNT +33%Si	66.1	866.7	587.6

Table 5.3 shows that with increasing silicon content in the composite anode, the initial capacity was increased. Also, the initial coulombic efficiency was improved with increasing silicon content. However, the capacity retention went down with increasing silicon content in the silicon-pristine CNT anodes: with 25% silicon, the charge capacity on the 20th cycle was 357mAh/g while it was 14 mAh/g for the sample with 54% silicon. With increased silicon content, the electrical conductivity was most likely decreased. For the anode with 54% silicon, it was thought that a large part of the silicon was not in good contact with the carbon nanotubes. The pulverized silicon during cycling further insulated the carbon nanotubes from the cell shell, resulting in dramatic capacity loss. When the arrays were first treated with a layer of amorphous carbon before silicon deposition, the cycling behavior was improved significantly. The carbon post-treated array anode containing 33% silicon retained a capacity of 587 mAh/g on the 20th cycle. Though the pristine array anode containing 30% silicon started with a slightly higher initial capacity, the charge capacity dropped to 373.9mAh/g at 20th cycle. It was assumed that with amorphous carbon deposited on surface of carbon nanotube array, silicon nano-particles attached to the surface more evenly and closely, which was confirmed by the SEM images.

6. Densified carbon nanotube array-silicon-carbon double shell structure preparation to improve lithium ion battery anode efficiency

6.1 Background

Depositing silicon on post-treated array improved the cycling behavior of the battery. However, the irreversible capacity in the first cycle needs to be minimized. The stability of the battery still needs to be improved and depositing a thin layer of carbon on the silicon layer should provide it with some protection [63] . Thus, there will be less SEI formation on the silicon surface, reducing the first cycle capacity fading. More importantly, the outer carbon shell can restrict the deformation of silicon during lithium intercalation, suppressing volume expansion [64]. At the same time, the outer carbon shell will contact with the battery shell instead of silicon, leading to much better electrical conductivity of the anode. The possibility of silicon dioxide formation, when the sample is removed from the CVD systems and exposed to atmosphere, will also be diminished.

6.2 Anode preparation

Silicon was deposited on chlorine post-treated array as in section 4 and 5. After the silicon deposition, another layer of amorphous carbon was deposited onto the array using the CVD system. The deposition conditions were 600sccm C_2H_2, 5 Torr and 760℃ for 5min. The as-prepared material was shear pressed, punched and assembled into coin cells by the same method described in section three.

6.3 Characterization

6.3.1 SEM

The morphology of the tri-layer composite was observed using SEM. The middle of the array cross section was closely examined as shown in Figure 6.1.

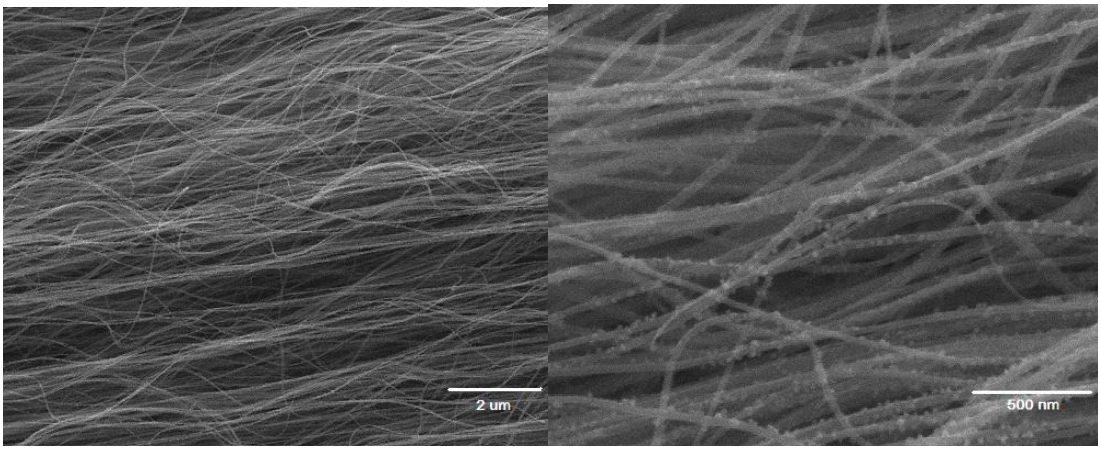

Figure 6.1 Composite CNT array (chlorine+-30%Si+carbon).

As seen in Figure 6.1, individual carbon nanotubes had relatively uniform silicon particles closely packed along the length of the tube. The morphology of silicon deposition was more uniform than pristine one. The tri-layer composite surface looked smoother than silicon-amorphous carbon post-treated one, which may be due to the coverage of amorphous carbon on silicon.

6.3.2 Raman Spectroscopy

Raman spectroscopy results of the top of the composite CNT array (chlorine+-30%Si+carbon) was shown in Figure 6.2.

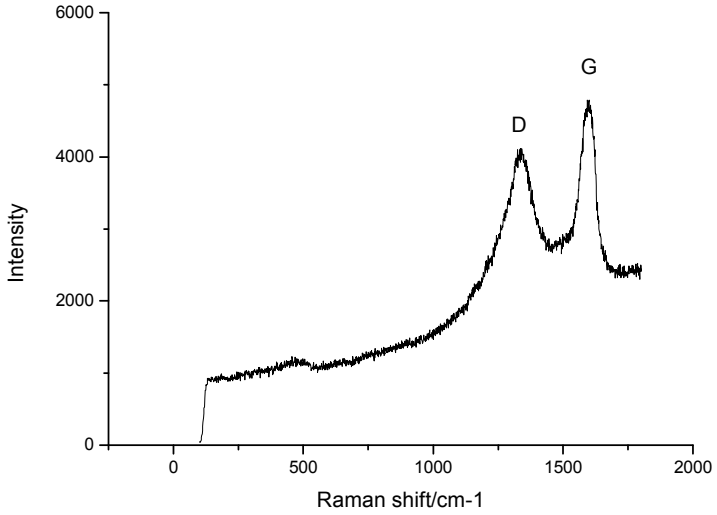

Figure 6.2 Raman spectroscopy composite CNT array (chlorine+-30%Si+carbon).

In the Raman spectroscopy results, there were peaks at at 1350 cm-1 and 1580 cm-1, which were corresponding to amorphous and graphitic carbon respectively. In contrast to Figure 5.1, no significant silicon peak (at 520 cm^{-1}) was observed in the plot. The lack of silicon peak on the top of the sample surface indicated a relatively uniform amorphous carbon coating on silicon.

6.3.3 EDS

During battery testing, some battery cells appeared to fail due to reactions with impurities in the anode. Though it was not certain if the impurities were introduced during material preparation or cell assembly, it would be better if the material was clean. Residual iron was cleaned from the array using the chlorine treatment. Iron reacts with chlorine according the equation $Fe+XCl_2=FeCl_{2x.}$ Iron chloride evaporates at temperatures lower than the temperatures used for the chlorine post treatment, thus, iron can be removed from

the CNT array while at the same time producing the active sites needed for uniform silicon deposition. The cleaning function of chlorine post-treatment was done under 760° C, 5 Torr and 400 sccm 0.5% Cl_2. EDS was used to examine the iron content in the samples (Table 6.1 and Figure 6.3). Unfortunately, the level of iron impurity was not known during the experiments conducted in sections 4 and 5 so the chlorine treatment was only used for silicon composite anode structures in this section.

Table 6.1 EDS data of sheer pressed carbon nanotube array sample.

Treatment / Element	Pristine	15min chlorine post-treated	30min chlorine post-treated
C	93.92	98.51	99.11
O	2.79	0.89	0.67
Fe	3.29	0.6	0.22
Total	100	100	100

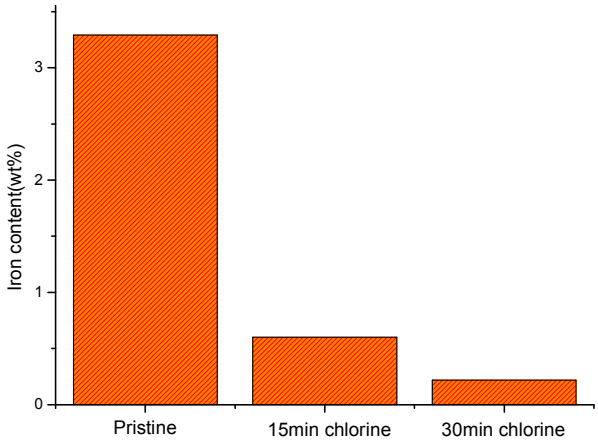

Figure 6.3 Comparison of iron content.

In Table 4.2 and Figure 4.4, the pristine carbon nanotube arrays contained about 3.3% iron, which came from the residual catalyst. After a 15 min chlorine post-treatment, the

iron content dropped to 0.6%, which was trace amount to the EDS detector. When the chlorine post-treatment time extended to 30min, the iron content decreased even further. In application for anode material cleaning, it is desirable to have a clean sample with a shorter post-treatment, since long treatment can damage the sample. So the relatively short 15 minutes chlorine post-treatment was recommended for practical use, with sufficient cleaning.

6.3.4 Electrochemical

The composite CNT array (chlorine+30%Si+carbon) anodes were cycled to test the electrochemical properties as shown in Figures 6.4 and 6.5.

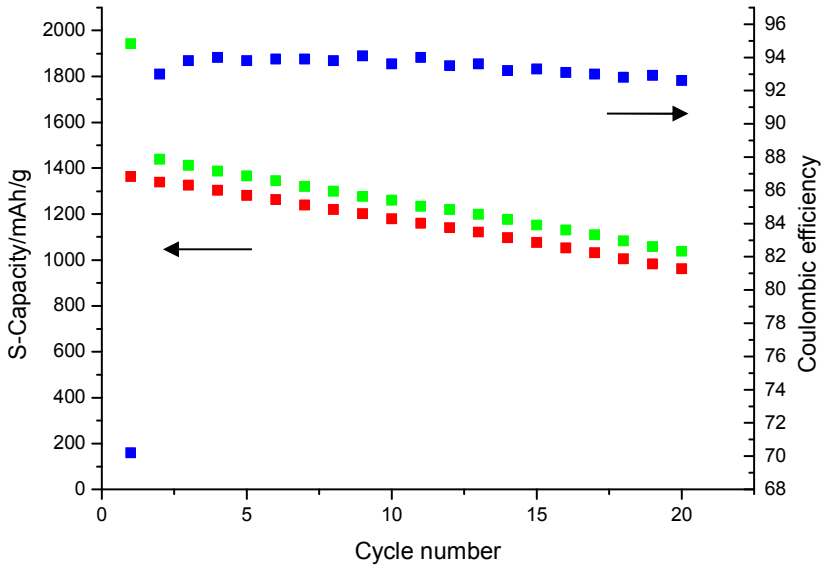

Figure 6.4 Composite CNT array (chlorine+-30%Si+carbon) anode.

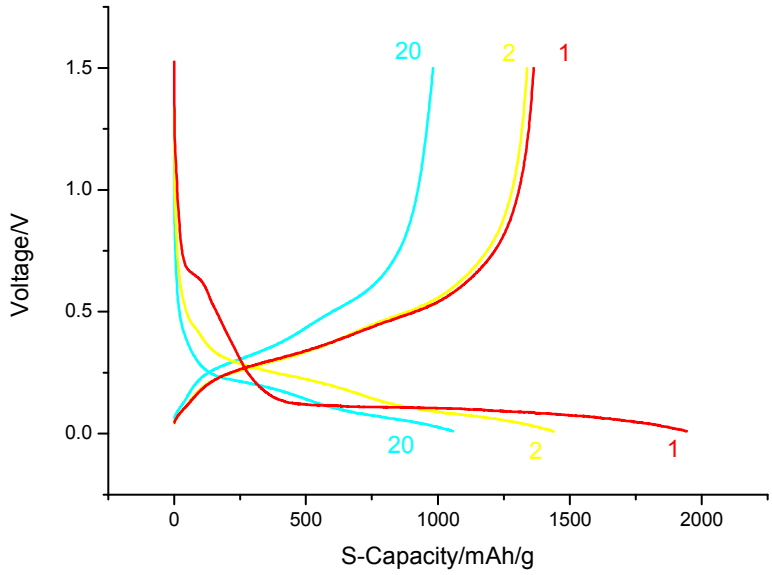

Figure 6.5 Voltage profile of composite CNT array (chlorine+-30%Si+carbon) anode.

For the composite CNT array (chlorine+30%Si+thermal) anode, the properties were good with high efficiency and better capacity retention, which may be attributed to better coherence of the structure and less iron impurity in the arrays. The overall capacity retention of the double shell anode was better. It was assumed that the amorphous carbon on top of silicon can help prevent the contact with electrolyte, reducing the formation of SEI layer on silicon, which improves the contribution of silicon to the capacity as well as the coulombic efficiency. Since the volume expansion of silicon during lithium insertion and extraction was compensated not only from carbon nanotubes but also from amorphous carbon, the cycling behavior of the anode was increased.

7. Discussion

The advantage of the vapor phase catalyst deposition method for producing carbon nanotubes is to grow highly aligned arrays of millimeter length in a short time. The optimization of growth conditions are crucial to obtain a high quality array. Under the optimized conditions, the arrays for lithium ion battery anodes have a relatively consistent length of about 1.5mm, which is critical for producing densified sheets of anode material and important for the consistency of electrochemical behavior.

Table 7.1 Comparison of properties of anodes.

	Initial coulombic efficiency(%)	First cycle charge capacity (mAh/g)	Capacity retention at 20th cycle (mAh/g)
CNT	30.9	102.9	103.6
CNT (Carbon+thermal)	34.3	143.9	169.1
Composite CNT (30%Si)	70.7	882.6	373.9
Composite CNT(Carbon+thermal+33%Si)	66.1	866.7	587.6
Composite CNT(chlorine+30%Si+ Carbon)	70.2	1363.2	982.2

By depositing silicon on carbon nanotube arrays, the capacity of carbon nanotubes was improved a lot with reduced irreversible capacity in the first cycle. The advantage of the

chemical vapor deposition of silicon is to form nano-sized particles penetrating the whole array. In Table 7.1, through depositing silicon on carbon nanotube arrays, the specific charge capacity in the first cycle was increased by eight to ten times. Also, the initial coulombic efficiency was improved by about two times. The reason for the capacity increase is the contribution from silicon. Compared with pristine carbon nanotube arrays, the coulombic efficiency of silicon coated arrays is about two times higher. The reason is that the silicon coating on carbon nanotubes limited the insertion and trap of lithium ions in graphene layers. The composite anodes with silicon on amorphous carbon post-treated arrays showed more stable cycling performance than the ones with silicon on pristine arrays. The amorphous carbon-silicon-chlorine post-treated carbon nanotube array anodes showed even higher capacity and cycling performance.

Theoretical capacity of the anode is calculated based on equation and summarized in Table 7.2:

$$C_{anode} = C_{Si} \times wt_{Si}\% + C_{CNT} \times wt_{CNT}\%$$

C_{anode} is theoretical specific capacity of anode; C_{Si} and C_{CNT} are theoretical specific capacity of anode respectively, where C_{Si}=4200mAh/g and C_{CNT}=144mAh/g for post-treated array and 104mAh/g for pristine array (The specific capacity of carbon nanotube arrays are averaged from data in this study since it varies from lab to lab).

Table 7.2 Comparison of actual capacities and theoretical capacities.

	Actual Initial capacity C_A (mAh/g)	Theoretical initial capacity C_T (mAh/g)	Ratio C_A/C_T
Composite CNT (30%Si)	882.6	1332	0.66
Composite CNT (Carbon+ thermal +33%Si)	866.7	1483	0.58
Composite CNT(chlorine+30%Si+ carbon)	1363.2	1365	0.99

Table 7.2 compares the actual and theoretical capacity of different composite structure containing about the same amount of silicon. A larger C_A/C_T ratio means that there was a larger silicon contribution to the capacity of the anode. The double shell structure has a ratio close to 1, which means the deposited silicon in this condition almost reaches the theoretical capacity 4200 mAh/g, partially due to the reduced SEI layer formation on silicon under amorphous carbon protection. Another reason for the increase in silicon contribution can be attributed to better electric contact provided by amorphous carbon. Instead of silicon in contact with the battery shell, amorphous carbon connects the shell with carbon nanotubes, leading to better overall conductivity. On the other hand, although capacity retention of silicon on post-treated array anode is much better than pristine array, the silicon contribution is still low due to SEI formation on silicon nano particles.

In the lab, the weight of the copper foil current collector (Fig7.1) is about 30mg. In this study, the weight of the anode was about 2.5mg. In other silicon-carbon composite anodes, the binder can takes 10%~15% weight percent of the anode [53]. The elimination of using current collector can improve the energy density of the anode by about 10 times.

Figure 7.1 Copper foil-most common current collector.

Table 7.3 presents the change of initial capacities change before and after including the weight of binder and additives in calculation. Table 7.4 compares the change of initial capacities before and after counting in the weight of current collectors. In the mixed CNT Si composite in table 7.3, silicon was deposited onto vertically aligned CNT first. Then the structure was destroyed and mixed with 50 wt% of binder and additives, resulting in a much lower actual capacity. The capacities of other composites with CNT also decreased in the calculation with considerable amounts of binder and additives. In table 7.4, the SiNWs on Cu anode had only a third of the capacity when adding in the weight of Cu collector. The capacity of commercial graphite anode also lost one fifth of the capacity due to the current collector. Since the anode in this study did not use binder, any binder or additives, the energy densities did not decrease from the perspective of the entire anode.

Table 7.3 Comparison of capacities based on active material+binder and additives

Composite Anode	Binder and additives wt%	Initial capacities (active material only) (mAh/g)	Initial capacities (active material+binder and additives) (mAh/g)
CNT (chlorine+30%Si+carbon)	0	1363.2	1363.2
Mixed CNT Si composite [50]	50	2050	1025
Mixed CNT, graphite and Si composite [66]	30	1800	1260
Randomly networked CNT in Si (1:9) [17]	15	2000	1700

Table 7.4 Comparison of capacities based on active material+current collector [67]

	Initial capacities (active matieral only) (mAh/g)	Initial capacities (active material+current collector) (mAh/g)
CNT (chlorine+30%Si+carbon)	1363.2	1363.2
SiNWs on Cu	3000	500
Metal oxide on Cu	900	600
Sn on Cu	600	354
Cu-Sn alloy	350	191
Mesocarbon composite	340	317
Commercial graphite on Cu	372	271

From the view of the complete battery cell system, according to a report from Center for Transportation Research in Argonne National Laboratory [16], the PVDF binder and the copper current collector for the anode together can account for as much as 12.8% weight

percent of the whole cell, as shown in Table 7.3. By eliminating the binder and current collector, the energy density of the cell can be increased by around 10%. It indicates that the anode structures in this study is very promising for potential applications and worth further investigation.

Table 7.5 Estimated material weight percent of typical Li-ion cells [16].

	High-Energy (100-A-h) Cell		High-Power (10 A.h) Cell	
Material/Component	Quantity (g)	Percent by Weight	Quantity (g)	Percent by Weight
Anode material (graphite)	563.6	16.4	14.1	4.3
Binder (PVDF)	69.7	2.0		
Current collector (Cu)	151.9	4.4	41.6	12.8

8. Conclusions

- Current collector free, binder free lithium ion battery anodes produced from densified, silicon coated, carbon nanotube arrays were studied in the research.

- Post-treatments decrease the G to D ratio of carbon nanotubes. Chlorine post-treatment is effective in removing the iron impurity in as-produced carbon nanotube arrays.

- Higher silicon content in the silicon CNT array composite results in faster fading during cycling. Among all anodes in this study, composite CNT array (chlorine+30%silicon+carbon) anode has the highest silicon contribution and best capacity retention with an initial capacity of 1363mAh/g and a capacity of 982mAh/g at 20^{th} cycle.

- The energy density of the current collector free, binder free silicon CNT composite anode is much higher than traditional anode, which is promising for future applications in portable equipment and vehicles.

9. Recommendations for future work

The study showed the great potential of densified silicon-CNT array anodes for lithium ion batteries. However, the cycling stability of anodes produced using this technology should be increased. The interface between silicon and carbon nanotubes needs to be further explored. Methods to improve the bonding and coherence of the composite structure should be developed. It is possible that some chemicals can be added during deposition to anchor silicon onto carbon nanotubes. Also, physical and chemical post-treatments of the composites may stabilize the structure to some extent. In addition, the morphology of deposited silicon can be further optimized, especially along the height of the array.

Though the double shell structure with amorphous carbon on top of silicon works better than previous anodes in the study, the conditions such as the deposition time and pressure need to be optimized. Once a thin the amorphous carbon covers the whole surface of each silicon particle, the SEI layer formation on silicon surface can be reduced. Carbon nanotubes and amorphous carbon together can provide silicon with ideal buffer to release stress built-up during strain changes. The cycling behavior will then be further improved with a decrease in irreversible capacity.

Another set of experiments should be conducted to purify the anode. Although iron can be cleaned through chlorine post treatment, other impurities such as silicon dioxide,

calcium and aluminum can be induced during handling, which may have some effect on the properties of the anodes.

In future studies, high rate performance of the silicon-carbon nanotube composite anodes should be explored. Due to the highly aligned structure through the anode thickness, these type of composite anodes are quite promising for high power batteries.

References

1. Landi BJ, Ganter MJ, Cress CD, DiLeo RA, Raffaelle RP. Carbon nanotubes for lithium ion batteries. Energy & Environmental Science 2009;2:638-54.

2. Lu X, Chen Z. Curved pi-conjugation, aromaticity, and the related chemistry of small fullerenes (<C60) and single-walled carbon nanotubes. Chemical Reviews 2005;105:3643.

3. Yu M, Funke HH, Falconer JL, Noble RD. High density, vertically-aligned carbon nanotube membranes. Nano Letters 2009;9(1):225-9.

4. Zhao H, Zhang Y, Bradford PD, Zhou Q. Carbon nanotube yarn strain sensors. Nanotechnology 2010;21(305502):1-5.

5. Gui X, Wei J, Wang K, Cao A, Zhu H. Carbon nanotube sponges. Advanced Materials 2010;22:617-21.

6. Zheng G, Hu L, Wu H, Xiec X, Cui Y. Paper supercapacitors by a solvent-free drawing method. Energy & Environmental Science 2011;4:3368-73.

7. Iijima S. Helical microtubles of graphitic carbon. Nature 1991;345:56-8.

8. Meyyappan M, Srivastava D. Carbon nanotube. IEEE Potentials 2000;August:16-8.

9. Yua Z, Chena D, Tøtdalb B, Zhaoc T, Daic Y. Catalytic engineering of carbon nanotube production. Applied Catalysis A: General 2005;279:223-33.

10. Inoue Y, Kakihata K, Hirono Y, Horie T, Ishida A. One-step grown aligned bulk carbon nanotubes by chloride mediated chemical vapor deposition. Applied Physics Letters 2008;92:213113-1,213113-3.

11. Kasavajjula U, Wang C, Appleby AJ. Nano- and bulk-silicon-based insertion anodes for lithium-ion secondary cells. Journal of Power Sources 2007;163:1003-39.

12. Fergus JW. Recent developments in cathode materials for lithium ion batteries. Journal of Power Sources 2010;195:939-54.

13. Arora P, Zhang Z. Battery separators. Chemical Reviews 2004;104:4419-62.

14. Aurbacha D, Talyosefa Y, Markovskya B, Markevicha E. Design of electrolyte solutions for li and li-ion batteries: A review. Electrochimica Acta 2004;50:247-54.

15. Lestriez B. Functions of polymers in composite electrodes of lithium ion batteries. Comptes Rendus Chimie 2010;13:1341-50.

16. Gaines L, Cuenca R. Costs of lithium-ion batteries for vehicles. ; 2000. Report nr ANL/ESD-42.

17. Zhang SS. A review on electrolyte additives for lithium-ion batteries. Journal of Power Sources 2006;162:1379-94.

18. Skundin AM, editor. The problem of carbon nanotubes using in lithium-ion batteries. Springer; 2008.

19. Yazami R. Surface chemistry and lithium storage capability of the graphite-llithium electrode. Electrochimica Acta 1999;45:87-97.

20. Whittingham MS. Inorganic nanomaterials for batteries. Dalton Transactions 2008:5424-31.

21. Yazami R. Surface chemistry and lithium storage capability of the graphite-llithium electrode. Electrochimica Acta 1999;45:87-97.

22. Ji L. Lithium alloy-carbon composite nanofibers for energy storage by electrospinning and carbonization. NCSU; 2009. 6 p.

23. Bradford PD, Wang X, Zhao H, Zhu YT. Tuning the compressive mechanical properties of carbon nanotube foam. Carbon 2011;49:2834-41.

24. Hao Z, Cao G, Wang Z, Yang Y, Shi Z, Gu Z. Carbon nanotube array anodes for high-rate li-ion batteries. Electrochimica Acta 2010;55:2873-7.

25. Zhang H, Cao G, Yang Y. Carbon nanotube arrays and their composites for electrochemical capacitors and lithium-ion batteries. Energy & Environmental Science 2009;2:932-43.

26. Guo-Tao Wu, Mao-Hui Chen, Guang-Ming Zhu, Jin-Kua You, Zu-Geng Lin, Xiao-Bin Zhang. Structural characterization and electrochemical lithium insertion properties of carbon nanotubes prepared by the catalytic decomposition of methane. Journal of Solid State Electrochemstry 2002;7:129-33.

27. Obrovacz MN, Christensen L. Structural changes in silicon anodes during lithium Insertion/Extraction. Electrochemical and Solid-State Letters 2004;7(5):A93-6.

28. Park M, Kim MG, Joo J, Kim K, Kim J. Silicon nanotube battery anodes. Nano

Letters 2009;9(11):3844-7.

29. Datta MK, Kumta PN. Silicon and carbon based composite anodes for lithium ion batteries. Journal of Power Sources 2006;158:557-63.

30. Eom JY, Park JW, Kwon HS, Rajendrana S. Electrochemical insertion of lithium into multiwalled carbon Nanotube/Silicon composites produced by ballmilling. Journal of the Electrochemical Society 2006;153(9):A1678-84.

31. Ji L, Zhang X. Evaluation of Si/carbon composite nanofiber-based insertion anodes for new-generation rechargeable lithium-ion batteries. Energy & Environmental Science 2010;3:124-9.

32. Lee H, Lee S. Carbon-coated nano-si dispersed oxides/graphite composites as anode material for lithium ion batteries. Electrochemistry Communications 2004;6:465-9.

33. Nanda J, Datta MK, Remillard JT, O'Neill A, Kumta PN. In situ raman microscopy during discharge of a high capacity silicon–carbon composite li-ion battery negative electrode. Electrochemistry Communications 2009;11:235-7.

34. Lee J, Bae J, Heo J, Han T, Cha NS. Effect of randomly networked carbon nanotubes in silicon-based anodes for lithium-ion batteries. Journal of the Electrochemical Society 2009;156(11):A905-10.

35. Wen ZS, Yang J, Wang BF, Wang K, Liu Y. High capacity silicon/carbon composite anode materials for lithium ion batteries. Electrochemistry Communications 2003;5:165-8.

36. Dimov N, Kugino S, Yoshio M. Mixed silicon–graphite composites as anode material for lithium ion batteries. Journal of Power Sources 2004;136:108-14.

37. Ng SH, Wang J, Wexler D, Chew SY, Liu HK. Amorphous carbon-coated silicon nanocomposites: A low-temperature synthesis via spray pyrolysis and their application as high-capacity anodes for lithium-ion batteries. The Journal of Physical Chemistry 2007;111:11131-8.

38. Kim H, Cho J. Superior lithium electroactive mesoporous si @ carbon core-shell nanowires for lithium battery anode material. Nano Letters 2008;8(11):3688-91.

39. Huang R, Fang X, Shen W, Zhu J. Carbon-coated silicon nanowire array films for high-performance lithium-ion battery anodes. Applied Physics Letters 2009;95:133119-1,133119-3.

40. Kima T, Mob YH, Nahmb KS, Oha SM. Carbon nanotubes (CNTs) as a buffer layer

in silicon/CNTs composite electrodes for lithium secondary batteries. Journal of Power Sources 2006;162:1275-81.

41. Arie AA, Vovk OM, Leea JK. Surface-coated silicon anodes with amorphous carbon film prepared by fullerene C60 sputtering. Journal of the Electrochemical Society 2010;157(6):A660-5.

42. Jung YS, Lee KT, Oh SM. Si–carbon core–shell composite anode in lithium secondary batteries. Electrochimica Acta 2007;52:7061-7.

43. Gao P, Fu J, Yang J, Lv R, Wang J, Nuli Y, Tang X. Microporous carbon coated silicon core/shell nanocomposite via in situ polymerization for advanced li-ion battery anode material. Electrochimica Acta 2007;52:11101-5.

44. Yoshio M, Wang H, Fukuda K, Umeno T. Carbon-coated si as a lithium-ion battery anode material. Journal of the Electrochemical Society 2002;149(12):A1598-603.

45. Dimov N, Kugino S, Yoshio M. Carbon-coated silicon as anode material for lithium ion batteries: Advantages and limitations. Electrochimica Acta 2003;48:1579-87.

46. Chandrashekar A, Ramachandran S, Pollack G, Lee J-, Lee GS, Overzet L. Forming carbon nanotube composites by directly coating forests with inorganic materials using low pressure chemical vapor deposition. Thin Solid Films 2008;517:525-30.

47. Wolf H, Pajkic Z, Gerdes T, Willert-Porada M. Carbon–fiber–silicon-nanocomposites for lithium-ion battery anodes by microwave plasma chemical vapor deposition. Journal of Power Sources 2009;190:157-61.

48. Chen P, Xu J, Chen H, Zhou C. Hybrid silicon-carbon nanostructured composites as superior anodes for lithium ion batteries. Nano Research 2011;4(3):290-6.

49. Wang Y, Li Y, Lu J, Zang J, Huang H. Microstructure and thermal characteristic of si-coated multi-walled carbon nanotubes. Nanotechnology 2006;17:3817-21.

50. Wang W, Kumta PN. Nanostructured hybrid Silicon/Carbon nanotube heterostructures: Reversible high-capacity lithium-ion anodes. ACSNANO 2010;4(4):2233-41.

51. Wang W, Epur R, Kumta PN. Vertically aligned silicon/carbon nanotube (VASCNT) arrays: Hierarchical anodes for lithium-ion battery. Electrochemistry Communications 2011;13:429-32.

52. Guo J, Chen X, Wang C. Carbon scaffold structured silicon anodes for lithium-ion batteries. Journal of Materials Chemistry 2010;20:5035-40.

53. Rong J, Masarapu C, Ni J, Zhang Z, Wei B. Tandem structure of porous silicon film on single-walled carbon nanotube macrofilms for lithium-ion battery applications. ACSNANO 2010;4(8):4683-90.

54. Kim S, Shim H, Lee JK. Electrochemical performance of silicon thin film anodes covered by diamond-like carbon with various surface coating morphologies. Journal of Solid State Electrochemstry 2010;14:1247-53.

55. Krishnan R, Lu T, Koratkar N. Functionally strain-graded nanoscoops for high power li-ion battery anodes. Nano Letters 2011;11:377-84.

56. Zhang T, Gao J, Fu LJ, Yang LC, Wu YP, Wu HQ. Natural graphite coated by si nanoparticles as anode materials for lithium ion batteries. Journal of Materials Chemistry 2007;17:1321-5.

57. Xie J, Cao GS, Zhao XB. Electrochemical performances of si-coated MCMB as anode material in lithium-ion cells. Materials Chemistry and Physics 2004;88:295-9.

58. Cui L, Yang Y, Hsu C, Cui Y. Carbon-silicon core-shell nanowires as high capacity electrode for lithium ion batteries. Nano Letters 2009;9(9):3370-4.

59. Katar SL, Labiosa AB, Plaud AE, Mosquera-Vargas E, Fonseca L, Weiner BR, Morell G. Silicon encapsulated carbon nanotubes. Nanoscale Research Letters 2010;5:74-80.

60. Cui L, Hu L, Choi JW, Cui Y. Light-weight free-standing carbon nanotube-silicon films for anodes of lithium ion batteries. ACSNANO 2010;4(7):3671-8.

61. Sinnott SB, Andrews R, Qian D, Rao AM, Mao Z, Dickey EC. Model of carbon nanotube growth through chemical vapor deposition. Chemical Physics Letters 1999;315:25-30.

62. Bradford PD, Wanga X, Zhao H, Maria J, Jia Q, Zhu YT. A novel approach to fabricate high volume fraction nanocomposites with long aligned carbon nanotubes. Composites Science and Technology 2010;70:1980-5.

63. Si Q, Hanai K, Imanishi N, Kubo M, Hirano A, Takeda Y, Yamamoto O. Highly reversible carbon–nano-silicon composite anodes for lithium rechargeable batteries. Journal of Power Sources 2009;189:761-5.

64. Hertzberg B, Alexeev A, Yushin G. Deformations in si-li anodes upon electrochemical alloying in nano-confined space. J AM CHEM 2010;132:8548-9.

65. Zhang Y, Zhang XG, Zhang HL, Zhao ZG, Li F, Liu C, Cheng HM. Composite anode material of silicon/graphite/carbon nanotubes for li-ion batteries. Electrochimica Acta 2006;51:4994-5000.

65. Zhang Y, Zhang XG, Zhang HL, Zhao ZG, Li F, Liu C, Cheng HM. Composite anode material of silicon/graphite/carbon nanotubes for li-ion batteries. Electrochimica Acta 2006;51:4994-5000.